MONTE CARLO SIMULATION OF ATMOSPHERIC NEUTRON TRANSPORT AT HIGH ALTITUDES USING MCNP

AFIT TECHNICAL REPORT: AFIT/EN-TR-90-5

Capt Donald R. Culp, USAF, B.S.
Lt David L. Monti, USAF, B.S.
Capt James R. Shoemaker, USAF, B.S.
Lt David Wesley, USAF, B.S.
LCDR Kirk A. Mathews, USN, Ph.D.

DEPARTMENT OF THE AIR FORCE

AIR UNIVERSITY

AIR FORCE INSTITUTE OF TECHNOLOGY

Wright-Patterson Air Force Base, Ohio

AFIT/EN-TR-90-5
August 1990

Accession For	
NTIS GRA&I	X
DTIC TAB	☐
Unannounced	☐
Justification	
By	
Distribution/	
Availability Codes	
Dist	Avail and/or Special
A-1	

MONTE CARLO SIMULATION OF ATMOSPHERIC NEUTRON TRANSPORT AT HIGH ALTITUDES USING MCNP

AFIT TECHNICAL REPORT: AFIT/EN-TR-90-5

Capt Donald R. Culp, USAF, B.S.
Lt David L. Monti, USAF, B.S.
Capt James R. Shoemaker, USAF, B.S.
Lt David Wesley, USAF, B.S.
LCDR Kirk A. Mathews, USN, Ph.D.

Approved for public release; distribution unlimited

PREFACE

This document reports upon research performed by four graduate students at the Air Force Institute of Technology. Captain Donald Culp, USAF, 1 Lt. David Monti, USAF, Captain James Shoemaker, USAF, and 1 Lt. David Wesley, USAF, concentrated upon different portions of the project; this report presents the research in a unified report.

This effort was part of an ongoing AFIT research project to develop effective computational methods for atmospheric radiation transport. The research was accomplished in Professor Mathews's course, NENG-601 (Research Apprenticeship), during the spring quarter of 1990. The goal of the course is to explore a real nuclear engineering problem in depth as a vehicle for developing engineering and research skills. Such a project is more closely led by the professor than a thesis project, while still providing substantial independence to the student, whence the title of the course.

This work was sponsored by the Air Force Weapons Laboratory; this AFIT technical report is intended to serve as a formal report to the sponsor. One of the goals of the project was to help the sponsors get started in performing this type of computation in house. We hope it provides the documentation necessary for further work to be accomplished on this topic starting from where we left off.

Table of Contents

Table of Figures

Table of Tables

ABSTRACT

Neutron transport calculations were performed using the Monte Carlo code, MCNP. The transport problem considered has a point source at high altitude (40 km). Since atmospheric density decreases with altitude, two-dimensional effects (cylindrical coordinates) can be important. Results were compared to those obtained with the SMAUG-II computer code, which performs mass-integral scaling of approximate fits to one-dimensional spherical discrete ordinates solutions. These comparisons show the importance of two-dimensional computations. The report discusses practical issues of applying MCNP to this problem, without code modifications and includes example input files for MCNP and for SMAUG-II.

EXECUTIVE SUMMARY

Computational modelling of neutron transport in the atmosphere is complicated by the variation of air density with altitude. A one-dimensional, spherical geometry solution can be applied to problems with a different density of the same medium, by scaling the $4\pi r^2$ fluence by ρr. However, this approach is strictly valid only in infinite media of constant density. As an approximation, it can be applied to a varying density medium by replacing ρr by $\int_0^r \rho(r')dr'$. This approach is known as "mass-integral scaling". This technique works reasonably well so long as the mean free path of the radiation is short compared to the distance over which the medium varies significantly in density. Shulstad [1] showed that, for point sources of fission or fusion neutrons, acceptable results could be obtained for source altitudes up to about 20 km. Above that height, one-dimensional calculations are inadequate.

Multidimensional calculations for each desired case are substantially more costly than one-dimensional mass-integral scaling schemes. Possibilities include diffusion methods, Monte Carlo transport modeling, and discrete ordinates (S_N) schemes. Shulstad developed a diffusion code which used a spatial mesh with curved, non-orthogonal coordinates, in which the cells form a rectangular matrix of data, and in which all cells are roughly equal in optical thickness. This method was effective, but is limited by the assumption of isotropic scatter (or at most, linearly anisotropic scatter) which is implicit in the use of the diffusion equation. An optimum approach, if we can make it work, would be to develop a discrete ordinates method with spatial and angular quadratures optimized for this problem, in which the spatial quadrature scheme would account explicitly for the variation of air density with altitude within each spatial cell. In order to benchmark the results of such a code, Monte

Carlo modelling will be needed. Indeed, if a specialized Monte Carlo code proved to be efficient enough, the discrete ordinates code could prove unnecessary.

The work reported here is a first step toward obtaining the needed Monte Carlo computations. An unmodified standard production code, MCNP, was used to solve air transport from a point source of neutrons. MCNP was selected because of its flexibility in representing the energy dependence of the neutron cross-sections, including multigroup (coarse mesh histogram), discrete (fine mesh histogram), and continuous (linear interpolation) representations. Cylindrical (r,z) geometry was used. Two test cases were attempted. With a large mesh and a source at 11 km altitude, very high cell importances were required for the cells most distant from the source. This problem never ran to completion; a smaller mesh was needed. With a mesh that was large in radius and height, but optically rather thin, the case with the source near 40 km altitude proved to be relatively straightforward. Results obtained were compared to corresponding results obtained using SMAUG-II, a mass-integral scaling code. The expected agreement at short ranges (and disagreement at longer ranges) was observed. The report provides practical details regarding employment of MCNP for this problem, including such areas as cross-section sets, variance reduction schemes, estimators, spatial meshing, problem definition, and input and output files. Details of the comparisons with mass-integral scaling results are also presented. The need for a histogram representation of the variation of air density with altitude appears to be the principal limitation to the use of MCNP for this problem. Future work should include efforts to modify MCNP to remove this limitation. Also, to reduce run times for this first effort, we omitted source and secondary photons from the calculations.

The goals accomplished during this effort included: getting MCNP up and running; learning to use it; developing input files which get it to solve this problem; evaluating the applicability and efficacy of the major variance reduction schemes and estimators (for this problem); and benchmarking the results with SMAUG-II.

1 Introduction

In 1976, Shulstad [1] investigated the adequacy of mass-integral scaling of one dimensional discrete ordinates calculations of coupled neutron-γ radiation transport from a point source in infinite homogeneous air as an approximation to the transport in the atmosphere (with its approximately exponential variation of air density with altitude). He compared various Monte Carlo results with the scaled one-dimensional results, and found good agreement at low altitudes (less than about twenty kilometers), but increasingly poor agreement at higher altitudes. He developed a specialized multigroup diffusion code, which used a two-dimensional, non-orthogonal, curvilinear coordinate system to maintain approximately equal optical thicknesses in each coordinate direction in each cell. His effort was successful, but his results are limited in accuracy by the assumption of at most linear anisotropy of scattering cross-sections which is intrinsic to the diffusion approximation.

With the increases in readily-available computing power which have been achieved in the fourteen years since Shulstad's work, we are revisiting this problem. The first step is to attempt to solve the problem efficiently with current production Monte Carlo software. We selected MCNP (described below) because of its flexibility in energy and cross-section representations. We used a special purpose mass-integral scaling code, SMAUG-II, provided by the Air Force Weapons Laboratory, for comparisons which confirm the accuracy of our results at close ranges, and which show the importance of two-dimensional effects at greater ranges and their dependence upon location of the field point with respect to the source point. Our goal in this effort was to ascertain whether MCNP could be used, as is, to provide computationally affordable solutions. We succeeded in obtaining reasonable solutions for the neutron fluences in regions within a few mean free paths of the source point. This report details these efforts and results. The computations were costly enough to make mapping the full field for a large selection of source altitudes expensive, although possibly not prohibitively so. However, direct Monte Carlo calculations for arbitrary source points and field locations would not be feasible as a subroutine to a parametric study, for example. Further work will be needed to customize MCNP for this problem and to evaluate the radiation field (including neutron-induced γ radiation) at much longer ranges. Later steps in this work may also include development of specialized discrete ordinates algorithms for solving this problem efficiently and without substantial ray effects.

1.1 Background

For low altitudes, the mean free path of neutrons and γ-rays is short compared to the scale height ("e-fold" distance) of the atmosphere, approximately 7 km. For these cases, the most widely accepted method in use today relies upon the simple technique of applying the results from a constant-density atmospheric model to that of the actual problem by means of scaling the $4\pi r^2$ fluence by the atmospheric mass between the source and field point locations. Shulstad concluded that this technique underestimates the radiation at very high altitudes and long ranges. This method and its limitations are discussed next.

1.2 Mass-Integral Scaling (MIS)

Radiation transport in air is described in detail by the Boltzmann transport equation. However, since the density of air varies in an exponential manner, numerical solutions to the Boltzmann equation in a variable density medium are generally not attempted. Instead, the determination of the radiation transport in air is computed through Monte Carlo simulations. These Monte Carlo simulations provide good answers for specific cases but there is a great computational cost associated with them. This high cost led to the development of quick running codes which use mass-integral scaling (MIS).

Mass-integral scaling is a technique in which the computed results of fluence or dose in a homogeneous system are used to approximate the fluence or dose in a variable density system such as the atmosphere. The computed results for the homogeneous system are easy to obtain computationally through discrete ordinates solutions to the Boltzmann transport equation. (In one-dimensional, spherical coordinates, discrete ordinates shows no ray effects and can be quite accurate.)

The point source radiation scaling law for two media of identical composition but different densities states that the same $4\pi r^2$ fluence is present at range r_A in medium A (with uniform density ρ_A), as is present at range r_B in medium B (with uniform density ρ_B), presuming that the same point source is present in each medium, and where the ranges are related by

$$\rho_B r_B = \rho_A r_A. \tag{1}$$

For mass-integral scaling, the scaling law is then extended to an approximation which relates the mass range in a homogeneous medium to the mass integral in a variable-density medium by

$$MI = \rho_H r_H = \int_0^{r_V} \rho_V(r')dr', \qquad (2)$$

where:

$\rho_H r_H$ is the mass integral in homogeneous medium,
r_V is the range in variable density medium,
$\rho_V(r')$ is the density as a function of position, and
MI is the mass integral.

Figure 1 shows the geometry used here. z is altitude; R is radius or "ground range", and r is range, or "slant range". In this notation, (R,z) is the standard cylindrical coordinate system. (The azimuthal angle is not needed here, due to symmetry.) We are usually concerned, however, with the spherical coordinate for range, r, since it determines the amount of spherical divergence. Since the density of air only varies with altitude, z, then the mass integral can be transformed to

$$MI = \int_{z_s}^{z_d} \rho(z)\frac{dz}{\sin\theta}, \qquad (3)$$

where:

z_s is the height of the point source of radiation,
z_d is the height of the "detector" (radiation field point of interest),
$\rho(z)$ is the air density as a function of altitude, and
θ is the source elevation angle (i.e., the angle between the horizontal and the direct path from source to detector).

For θ near zero, the change in altitude is approximately zero. Therefore the density is nearly constant along the direct path and the mass integral is simply the homogeneous mass range, computed using the density at the average altitude, $(z_s+z_d)/2$.

Note that, using an assumed exponential atmosphere, the mass integral can be obtained by analytic integration in equation (3), giving (for θ not too close to zero):

$$MI = \rho_0 \frac{7\text{km}}{\sin\theta}[\exp(-z_s/7\text{km}) - \exp(-z_d/7\text{km})], \qquad (4)$$

or (for θ close to zero):

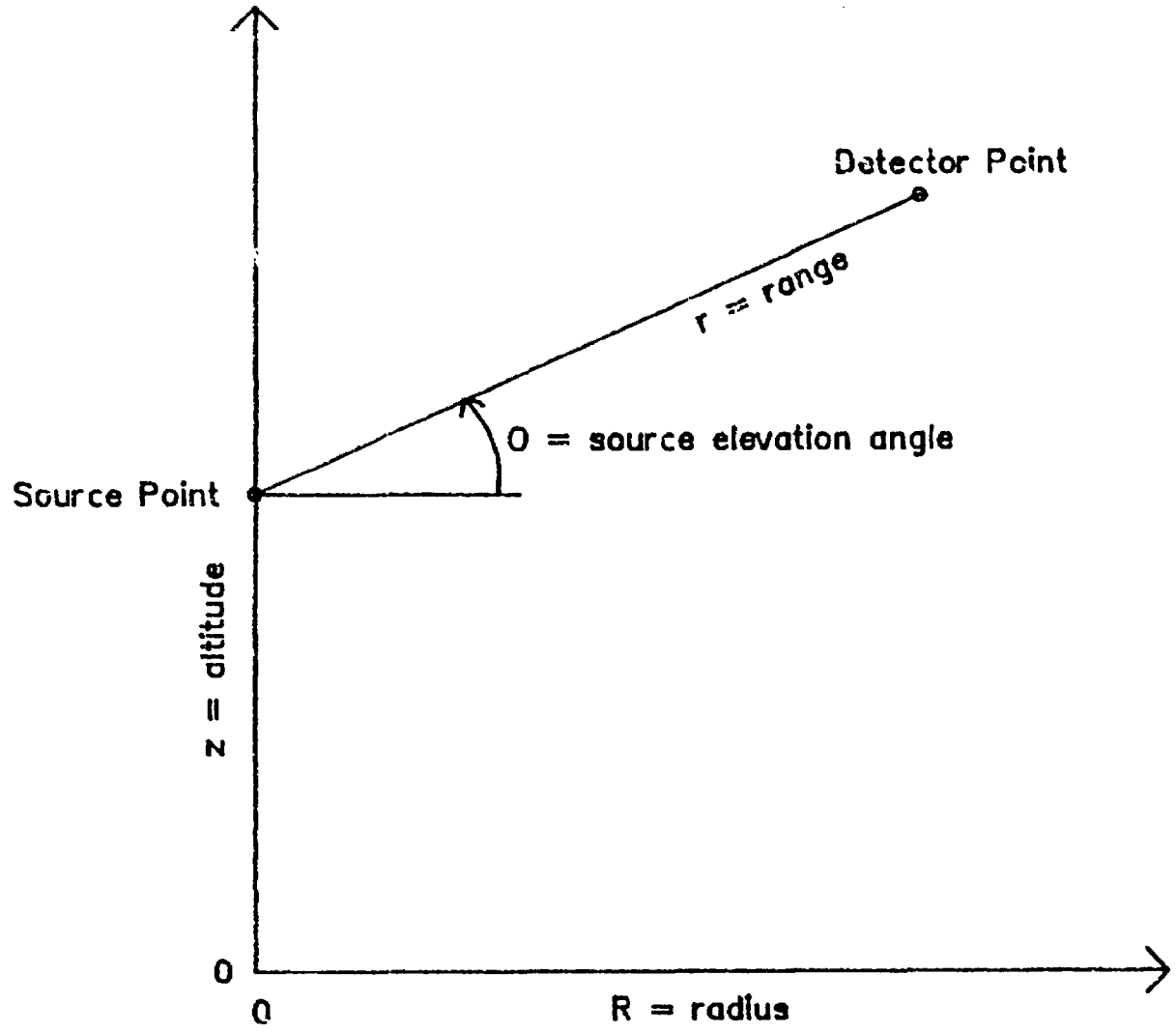

Figure 1 Geometry

$$MI \approx r\rho_0 \exp\left(\frac{-(z_s + z_d)/2}{7\,\mathrm{km}}\right). \qquad (5)$$

However, these solutions for mass integral (equations 4 & 5) were not used, since SMAUG-II computes them using a more accurate fit to $\rho(z)$.

The significance of the mass-integral scaling approximation is that once the mass integral is determined, the approximate solution can be found for the equivalent mass range in a homogeneous medium. Since the solutions in homogeneous media can be calculated in advance, and approximated by empirical fits or table interpolations, the computational effort for codes such as SMAUG-II is minimal.

1.3 SMAUG-II

SMAUG-II [2] is a computer program written in FORTRAN which computes the neutron and γ radiation from a point source of neutrons and γ-rays in the atmosphere, using a 58 energy group data base (37 neutron and 21 gamma). Required inputs to the code include the source strength, neutron and gamma source spectra, source altitude, and range (or radius, see figure 1) and altitude of the field point of interest. Outputs from SMAUG-II include (free-field) neutron and γ fluences, energy fluences, mean energies, energy spectra, and absorbed tissue and silicon doses at the detector.

The MIS employed by SMAUG-II relies upon discrete ordinates calculations of neutron and gamma transport in a homogeneous system. The code bases its calculations on a set of 1711 empirical transmission functions which are least squares fits to the results of neutron and γ-ray transport calculations from ANISN, a one-dimensional discrete ordinates code for calculating transport in a homogeneous system. The DLC-31 multigroup cross section set from Oak Ridge National Laboratory (ORNL) was used in those calculations. Also, the air composition was 79 percent nitrogen and 21 percent oxygen at a density of 1.11 mg/cm^3.

The empirical transmission function, $T(X)$, used to fit each source group to receiver group combination as a function of mass integral in air, is

$$\ln[T(X)] = C_1 X + C_2 X^2 + C_3 \ln(X) + C_4 \sqrt{X} + C_5 X^{1/3} + C_6 X^{3/2} + C_7. \qquad (6)$$

where C_1 through C_7 are least squares fit coefficients, and X is the mass integral.

The fitting process resulted in 1711 7-constant fits which reproduce (to sufficient accuracy) the ANISN results without the need for a lookup table. These results are all given as the $4\pi r^2$ fluence (or dose) per source neutron for the equivalent homogeneous system. The result is then divided by $4\pi r^2$, where r is the range between the source and field points. Finally, the result is multiplied by the number of source neutrons to get the fluence or dose for the variable density atmosphere.

SMAUG-II claims to be valid for all situations where both the source and the receiver are at least 500 meters above the ground, below a maximum altitude of 20 kilometers, and separated by a mass-integral of less than 1000 g/cm^2. These limitations are a problem inherent in mass-integral scaling and will be explored next.

1.4 Problems with MIS and SMAUG-II

Mass-integral scaling was derived from the Boltzmann transport equation by Zerby [3] and from the diffusion equation by Shulstad [1]. Furthermore, Shulstad developed a specialized multigroup diffusion code for the problem considered here and demonstrated that, for high enough altitudes, mass-integral scaling is inaccurate. Both authors show that this scaling is an approximation based on the assumption that the scattering and the geometric divergence can be separated. Mass-integral scaling is strictly correct only in a uniform homogeneous atmosphere (whence the one dimensional spherical ANISN calculations) but is only an approximation in the real case. The following example will illustrate this.

Consider two detectors, one above a given point source, the other below. If they are both at the same mass-integral, then the range to the upper detector will be greater than the range to the lower one, because of the decrease in air density with increasing altitude. We can illustrate the result by expressing it in terms of a broad beam attenuation problem using build-up factors, such as

$$4\pi R_{down}^2 F = S \times BUF_{down} \times \exp\left(-MI\frac{\sigma}{\rho}\right)$$
$$4\pi R_{up}^2 F = S \times BUF_{up} \times \exp\left(-MI\frac{\sigma}{\rho}\right). \qquad (7)$$

where:

F = Fluence,
BUF = Build Up Factor, and
S = Source Strength.

Using the MIS approximation, we find that

$$4\pi R_{down}^2 F_{down} = 4\pi R_{up}^2 F_{up}. \tag{8}$$

Therefore,

$$S \times BUF_{down} \times \exp\left(-MI\frac{\sigma}{\rho}\right) = S \times BUF_{up} \times \exp\left(-MI\frac{\sigma}{\rho}\right). \tag{9}$$

which means that BUF_{up} and BUF_{down} would have to be equal. However, a two dimensional transport or diffusion calculation would show that this is not the case. The upper detector would have a smaller build up factor because the air is less dense causing fewer scatters, and if the detector is high enough, there will be a significant number of particles that will simply leak out of the top of the atmosphere instead of scattering and contributing to the build-up.

Mass-integral scaling was evaluated by Shulstad using a special form of diffusion theory on a 2 dimensional non-orthogonal coordinate system. This coordinate system was developed to take into account the variable density nature of the atmosphere. The results of his evaluation were bench marked against Monte Carlo calculations and demonstrated that MIS resulted in errors of less than 20% for altitudes between 1 and 10 kilometers, and out to mass integrals of 220 g/cm^2. He found significant errors at altitudes greater than that because of the leakage out of the top of the atmosphere which was not accounted for by MIS.

A purpose of this project was to determine the error of SMAUG-II at elevations above 20 kilometers by comparing SMAUG-II approximations with Monte Carlo results at these higher altitudes. Two obstacles with the SMAUG-II code had to be overcome: one was a limit on the maximum altitude of 25 kilometers and the second was a limit on the maximum mass integral of 1000 g/cm^2. The SMAUG-II programmers put bounds on the input values to limit the use of the code to within the region where it should be reasonably accurate, but we needed to defeat these protections in order to see how inaccurate the code might be. The altitude problem was solved by changing the constant ALTMAX in the subroutine SMEXE from 25000 to 60000 (meters). The value of 60000 was chosen because that is the largest number that can be used for determining the mass integral as it is implemented in the code. The limitation on mass

integral turned out to be a hindrance only at low altitude which wasn't as important to the problem, therefore no attempt was made to increase it.

1.5 Approach to Problem

The approach to the problem of comparing high altitude SMAUG-II calculations to Monte Carlo calculations was along two lines. One was to try to validate SMAUG-II at low altitude where the results are supposed to be accurate to within 20%. Another was to compare SMAUG-II and MCNP results for a high altitude source point.

1.5.1 Validation

The test for validation consisted of examining the radiation from a point source at an altitude of 11 kilometers. The area which was to be analyzed extended out several kilometers and will be described thoroughly in a later section. The only problem from the SMAUG-II code was that some of the points which were to be tested were over the 1000 g/cm^2 mass integral limit. This was not significant though because it was not necessary to get data for SMAUG at every point that the Monte Carlo calculations would get data. As long as SMAUG-II could generate enough points for verification, then the 1000 g/cm^2 limit did not matter. As it turned out there were greater problems with using the Monte Carlo code which prevented the validation at lower altitude from being successful. This will also be explained in a later section. (A note in hindsight: since SMAUG-II was expected to be accurate only out to about 220 g/cm^2, the region for which calculations were attempted was needlessly large. This was the real reason the calculations were not successful.)

1.5.2 Comparison

The comparison test consisted of examining a point source at an altitude of 40.05 kilometers. The area of analysis will also be described in detail in a later section. The cells that the Monte Carlo code used extended as high up as 300 kilometers, but this did not affect the ability of SMAUG-II to provide comparison data at altitudes below 60 kilometers. The results were used for comparisons of fluences at constant ranges and of fluences at constant mass-integrals. In contrast to the low altitude test, the high altitude test used a maximum mass integral of approximately 14 g/cm^2. Again, the detailed results will be presented in a later section. Although it would have been more revealing to include a larger region, with mass integrals up to about 220 g/cm^2, this effort was restricted to demonstrating the methodology. Future efforts may succeed in increasing the ranges as desired.

1.6 Expectations

There were several expectations for the results of this comparison. The first expectation was that, at small ranges, the results of SMAUG-II and Monte Carlo should be nearly the same. This is because at small enough range in thin air, we should only see spherical divergence. Our results show this to be fairly accurate. Another expectation was that slightly farther out and co-altitude with the source, SMAUG-II should initially over predict because it fails to account for the magnitude of the leakage of radiation out the top of the atmosphere. In fact, the over prediction should get worse with increasing downward angle from the source, since the diffusion of the particles moves them away from these more dense areas up into less dense areas. Our results also showed this effect.

At some point it was expected that some of the particles which scattered upward may scatter down again after only a few scatters. But, because of the length of mean free path at the higher altitude, they would not reappear in our areas of interest for 10's of kilometers from the source. This would cause SMAUG-II to under predict the Monte Carlo results. This phenomena was not seen in our problem but there is a good reason why. In homogeneous air, the $4\pi r^2$ fluence increases with the mass integral (due to buildup of scattered radiation) until it peaks at a mass integral of about 30 g/cm^2; then it decreases, (due to absorption) reaching its original value at about 80 to 100 g/cm^2, and continues to decrease at even greater ranges. The area of this peak is the area where the build up factor is greater than one. This is why SMAUG-II is over predicting in this area. In order to reach an area where SMAUG-II under predicts, it may be necessary to go out as far as 60 g/cm^2, but for field points co-altitude with the source, that mass integral corresponds to a range of over 140 kilometers. The radiation intensity at such ranges may be negligible; in any event, we did not attempt to use such a large computational region for the Monte Carlo simulations.

Overall, SMAUG-II offered no surprises. Presentations of data in later sections will show that SMAUG-II behaved in the anticipated manner. Future work in this area may lead to the development of suitable correction factors.

2 Project Goals and Approach

The overall objectives of the project are as follows:

1. Using Monte Carlo simulations, generate a collection of benchmark results for a limited set of source height and field point locations, or if possible, to create multidimensional maps of the radiation distribution as a function of source height.

2. In anticipation of limited practicality of Monte Carlo simulation, generate multidimensional discrete ordinates (Sn) solutions to the problem.

The objectives for this particular study were as follows:

1. Compare Monte Carlo results with SMAUG-II results to evaluate the efficacy of Monte Carlo simulation for this problem and to assess the relative applicability of both methods.

2. Gain insight into the complexity of computationally modeling this problem and the difficulties in generating results for the benefit of subsequent studies.

The initial approach decided upon for this project was to use Monte Carlo simulation to try and map out the nuclear radiation distribution in three dimensional space which results from a point source. This was to be accomplished by use of an existing production code called Monte Carlo Neutron Photon (MCNP). The MCNP results could then be compared with those from SMAUG-II for identical source height and field point locations.

If the Monte Carlo results achieved acceptable resolution without excessive computer run times, then the data could simply be tabulated or mapped out graphically for various source heights; this would eliminate the need for the mass-integral scaling technique for this problem. But if this mapping out of the problem proved not to be practical, then MCNP would be used in an attempt to benchmark a few source height and field point location combinations by optimizing the computational variance reduction methods to get the best answer for each such combination. These benchmark cases could then be used to test the results from some other modeling technique, such as discrete ordinates. The benchmark cases are divided into two classes (high-altitude and low-altitude point source simulations) due to the great differences in modeling radiation transport at low altitudes versus high altitudes.

3 MCNP Code

MCNP [4] is a general-purpose, generalized-geometry, time-dependent, coupled neutron/photon Monte Carlo transport code developed by Los Alamos National Laboratory. It solves neutral particle transport problems and can be run in any of three modes; neutron transport only, photon transport only, or combined neutron/photon transport, in which the photons are produced by neutron inelastic interactions. (See Reference 2)

The user creates an input file that is read by MCNP. This file contains information about the problem in areas such as: the geometry specification, description of the materials, which cross-section evaluations to use, the location and characteristics of the radiation source, the type of answer or tallies desired, and any variance reduction techniques to be used. Examples of the input files used in this project are included in Appendix A, including explanatory remarks. (A summary of results is presented in Appendix B; tables of atmospheric number densities are provided in Appendix C.) The remainder of this section details the geometric specifications used to define the problem and how the various parameters of MCNP were tailored to this problem.

3.1 Assumptions and Approximations

1. Due to time constraints and the relatively short range of the initial photon radiation, only the coupled neutron/photon transport mode of MCNP was employed.

2. We did not address any time-dependence in the problem; instead, we generated neutron and energy fluence calculations only.

3. The model of the atmosphere we used was only made up by nitrogen and oxygen. Their relative abundances were 79% nitrogen and 21% oxygen. Since argon makes up most of the secondary elements in air and its nuclear cross-section of interaction is about that of nitrogen and oxygen, its contribution was taken as negligible. Also, we were unable to access the cross-section data with photon production for argon.

4. The air density changes with altitude, but the relative elemental mix was kept constant (79% nitrogen and 21% oxygen) up to 100 kilometers. This ratio varies by only a few percent over that altitude range. The actual number densities with altitude can be found in Appendix C, as provided by the Weapons Laboratory and based upon the U.S. Standard Atmosphere (1962) and CIRA models (1965).

5. The air density variation was analytically approximated by an exponential density profile in which there is an e-fold decrease in density every seven kilometers in altitude. In addition, the discretization of the atmosphere into layers of constant density introduced "stair-step" discontinuities in the air density profile.

3.2 Neutron Source Spectra

A generic mixed fission/fusion source spectrum was used for the high and low altitude problems. In order to perform accurate comparisons of results between SMAUG-II and MCNP, the same generic thermonuclear source spectrum was used in both

computer codes. The data provided by the Weapons Laboratory included a 37-group neutron spectrum (in file TNS.NEV) and a 21-group photon spectrum (in file EXP.GAM), ranging from sub-thermal energies to 14.2 MeV for the neutrons and 14 MeV for the photons. Only the neutron spectrum was used in the problem since using a coupled neutron/photon source spectrum would have increased run times. (Later efforts may include source photons.) In addition, at low altitudes, the source photons are attenuated in short distances, so the secondary photons (from inelastic scatter of neutrons and from neutron capture) are the dominant contribution.

The neutron thermonuclear source spectrum energy bin probabilities had been previously normalized to one, thus the spectrum could be directly input into the MCNP input file ("INP") with no further modifications. The source spectrum specifications within the "INP" file are given in Appendix A. The units for this spectrum are "neutrons per MeV per source neutron".

3.3 Cross Sections

The MCNP code package includes numerous libraries of nuclear data tables which contain neutron and photon cross-sections [5]. Various classes of nuclear data tables exist for MCNP. These include: (1) continuous-energy neutron interaction data, (2) discrete reaction neutron interaction data, (3) multigroup neutron interaction data, (4) continuous photon interaction data and (5) multigroup photon interaction data. In neutron-only and coupled neutron/photon problems, one continuous-energy, multigroup or discrete reaction neutron interaction table is required for every element in the problem. Likewise, one photon data table is required for every element in a coupled neutron/photon or photon-only problem.

Each library contains data processed from a different source of evaluated nuclear data files, such as ENDF/B-V, ENDL85 and PERMAFILE. Los Alamos is continuously replacing obsolete cross-section data from older sources. The input file for MCNP not only identifies the elements and isotopes for a problem, but also allows for the cross-sections from a specific library to be called out. Each nuclear data table is identified by a ZAID. The general form of a ZAID is ZZZAAA.nnX, where ZZZ is the atomic weight, AAA is the atomic number, nn is the evaluation identifier, and X indicates the class of data. For example, 7014.04D calls out nitrogen-14: the D is for discrete reaction cross-sections, and 04 identifies library D9 which is based upon ENDF/B-IV source file and includes photon production cross-sections. A 7014.50M calls out the multigroup cross-sections found in library MGXSNP1.

MCNP first accesses a consolidated reference file, called XSDIR, which provides the address for each ZAID called out in the input file. For more detail concerning cross-sections and MCNP, see the MCNP Users Manual, Reference 2.

3.3.1 Neutron Cross Sections

The primary source for MCNP neutron interaction data is the ENDF/B system. The most recent cross-sections in MCNP libraries are from ENDF/B-V Revision 2, but new MCNP interaction data is expected in the near future when Los Alamos releases data processed from ENDF/B-VI.

Data on the MCNP neutron interaction tables include cross-sections and much more. For a continuous-energy table, the cross-sections for each reaction are given on one energy grid, which is dense enough that linear interpolation between points reproduces the evaluated cross-sections within a tolerance that is generally one percent or less. The resulting energy grid may contain as few as around 250 points (for H-1) or as many as around 22,500 points (for Au-197).

Angular distributions of scattered neutrons are included for all nonabsorption reactions. When tables include data for secondary photon production, this data is presented as photon production cross-sections and photon angular distributions. All angular distributions are approximated in MCNP by equally probable cosine bins.

Discrete reaction tables are identical to the continuous-energy tables except that in the discrete reaction tables all cross-sections have been averaged into 262 groups. The averaging was done with a flat weight function. This is not a multigroup representation; the cross-sections are simply given as histograms rather than as continuous curves.

The multigroup tables have been derived from the same sources as the other neutron interaction tables, but the data has been collapsed into 30 energy groups. Most multigroup tables include photon production data in the same manner as the other table types.

3.3.2 Photon Cross Sections

The photon interaction tables are based upon the ENDL system. Cross-sections are given for coherent scatter, incoherent scatter, pair production and photoelectric effect. The form of the ZAID is ZZZ000.nnP for continuous-energy cross-sections and ZZZ000.nnG for multigroup photon cross-sections. For a neutron-induced photon problem, entering ZZZAAA.nnC or ZZZAAA.nnM for neutrons will cause automatic use of ZZZ000.nnP or ZZZ000.nnG, respectively, for photons.

Energy grids are tailored for each element and contain 40-60 points. Log-log interpolation is used to determine cross-sections between adjacent energies. Photon tables also include information pertaining to the direction and energy of scattered photons. The multigroup photon cross-sections have been collapsed into 12 energy groups. See Reference 2 for the multigroup energy spectrum.

3.3.3 Cross Sections Used

The majority of the continuous and discrete data libraries were available with the MCNP code for this project. These library files had been loaded onto the AFIT computer at the same time as the source code. However, not all of the data had been loaded, including the cross-sections for argon which contained secondary photon production information. Therefore, a coupled neutron/photon problem in the continuous-energy or discrete mode could not be conducted if the problem contained the element argon. Since the total cross-section for argon is on the same order as nitrogen and oxygen, and since argon makes up no more than one percent by volume of air, we excluded argon from the problem with a negligible increase in error anticipated.

The Weapons Laboratory provided a copy of the multigroup data library but we were unable to get MCNP to read data from the file. It appeared to be some sort of format problem between MGXSNP1, XSDIR, MCNP and perhaps even the computer operating system. Los Alamos is providing additional copies of XSDIR and MGXSNP1. It was initially planned to use the multigroup cross-sections in order to reduce run times and to allow a more direct comparison with a discrete ordinates solution. All calculations presented in this report were generated using discrete reaction cross-sections, rather than continuous-energy, in an effort to reduce computing times.

However, later calculations using the continuous-energy cross-sections demonstrated an insignificant difference in run time and the differences between results were within statistical uncertainties. This is due to the relatively simple behavior of the neutron cross-sections for nitrogen and oxygen with energy; it requires about the same number of data points to construct these cross-sections in both continuous and discrete modes.

3.4 Varying Atmospheric Density

The great variation of air density with altitude is the very reason why this is a nontrivial problem. The density of the atmosphere is approximately exponential; we assumed that this relationship was exact, i.e.,

$$\rho(z) = \rho_0 \exp\left(\frac{-z}{7\text{km}}\right). \qquad (10)$$

So for a problem defined over hundreds of kilometers in altitude, there are extreme differences in air density and therefore in the distances of radiation transport. For example, a 2 MeV neutron has a mean-free-path for collision at sea level of approximately 120 meters, while at forty kilometers altitude the mean-free-path is almost 40 kilometers and at 100 kilometers altitude it is essentially infinite compared to the dimensions of the atmosphere. In reality the atmospheric density profile is not exactly exponential, but this approximation is analytically straight-forward and should not introduce enough error to invalidate our insights and conclusions regarding the practicality of using Monte Carlo simulation for this problem. In any event, MCNP cannot represent this exponential variation explicitly; a histogram approximation using a spatial mesh of constant-density cells is necessary.

Table 1 was devised in order to help in the set-up of the geometries for this project. Only the interaction cross-sections for nitrogen and oxygen were used for neutrons and the total attenuation coefficient for air was used for photons. The mean-free-paths are given at sea level, but can be easily scaled to the altitude of interest using the seven kilometer rule.

Table 1
Radiation Mean-Free-Path at Sea Level

ENERGY	Neutron MFP	Photon MFP
0.025 eV	18 m	
1 keV	28 m	
10 keV		1.5 m
100 keV		50 m
2 MeV	120 m	150 m
10 MeV	145 m	385 m

The following sections explain the necessity to divide the geometry of the problem into cells of finite volume in order to implement the variance reduction methods. The other prime reason for this is that MCNP does not allow for a density gradient across cells, so many cells are required to represent the atmosphere. In order to properly represent the average air density for each cell (so as to conserve the mass of atmosphere within each cell), we integrate the exponential air density profile over the height of a cell to obtain

$$\bar{\rho} = \rho_0 \frac{7\,\mathrm{km}}{z_u - z_l}\left[\exp(-z_l/7\,\mathrm{km}) - \exp(-z_u/7\,\mathrm{km})\right], \qquad (11)$$

where:

$\bar{\rho}$ is the average density in the cell of interest,
ρ_0 is the air density at sea level,
z_u is the height of the upper cell boundary, and
z_l is the height of the lower cell boundary.

Because of the great variation of air density, these cells are not all the same size; they are much smaller at low altitudes than at high altitudes. The shallower or smaller the cells in height, the less coarse the air density profile. This equation was only used to model the atmospheric density up to 100 kilometers. Above that, the values from Appendix C were integrated numerically to obtain cell average densities.

3.5 MCNP Variance Reduction

Apart from the MCNP code documentation, LA-10363-MS [6] provides a very useful tutorial on the employment of variance reduction schemes in MCNP. The specific techniques we used (or tried to use) are discussed briefly next.

3.5.1 Geometric Splitting/Russian Roulette

Geometric splitting/Russian roulette is the most widely used variance reduction technique used in Monte Carlo analysis. It is the most effective first step in obtaining substantial gains in efficiency. This variance reduction technique was chosen for this problem for several reasons, the most important reason being lack of particle penetration, especially at low altitudes.

At low altitudes, (ground level up to several kilometers) the air is dense enough that the mean free path of neutrons is on the order of a few hundred meters. When defining a geometry which is tens of kilometers in diameter and in height, the direct path from the source to the detector will be approximately 10-20 mean-free-paths in length, and will decrease with increasing altitude. Clearly, penetration problems can arise for both the neutrons and photons when transporting these particles from the source to the detector.

At high altitudes, the medium is less dense, and the mean free path for the neutrons is on the order of kilometers instead of meters, and thus particle transport occurs with less need for splitting/Russian roulette.

In order to transport these particles through a relatively dense medium, splitting surfaces must be created within the geometry, allowing particle penetration by the creation of several particles with reduced weights at each boundary crossing. Particles that have small weights relative to the local cell will be Russian rouletted. The ultimate goal is to maintain an even particle population in each cell with each cell having a different average weight. This insures a more even statistical contribution from each cell. Details of the geometric splitting/Russian roulette variance reduction technique can be found in the MCNP manual, Chapter 2, page 123.

For both the high altitude and low altitude problems, the general procedure used in obtaining appropriate weights was as follows:

1. divide the geometry into cells;
2. assign initial importances to these cells;
3. run a few thousand particles with no tallies;
4. for each cell, calculate a new importance value (using the results in Table 126 of the MCNP output file) as the ratio of the population in the source cell to the population in the cell;
5. assign the new importances to these cells;
6. run a few thousand particles; and
7. repeat until the population and/or collisions in each cell is approximately the same for all cells.

Note that it is customary to assign a neutron/photon importance of 1 to the source cell.

This technique was successful in the high altitude problem, where adjacent cell importance ratios were low compared to the low altitude problem. Even though the total number of cells in both problems was approximately the same, the reduced splitting in the high altitude problem resulted in much shorter run times. For the low altitude problem, the extremely high cell importances (on the order of 5000 at some remote cell locations relative to the source location) resulted in excessive run times. Using a practical limit of 200 cells, no improvement was possible in reducing the cell thickness for better importance sampling.

3.5.2 Weight Window

The weight window variance reduction technique is a space-energy-dependent splitting and Russian roulette technique. Details can be found in the MCNP manual, Chapter 2, page 140. An attempt was made to invoke the weight window technique in

order to reduce the number of cells required and to counteract some of the penetration problems present at low altitudes using geometric splitting/Russian roulette. Some major advantages of the weight window technique are as follows:

1. weight window is space-energy dependent; geometric splitting is space dependent only,
2. weight window will discriminate on particle weight before deciding action; geometric splitting is done regardless of particle weight, and
3. weight window does not require splitting surfaces, and can be applied at surfaces, collision sites, or both; geometric splitting can only be applied at surfaces.

Unfortunately, the successful application of the weight window technique demands considerable user understanding and intervention. Entering weight window parameters such as energy and importance cut-offs and weight window widths can be tricky, and if incorrect, can be difficult to improve if the behavior of the particle energy and importance across cells is not well known. The internal weight window gererator within MCNP is designed to aid the user in generating weight window importance functions which would otherwise be found from guessing, intuition, experience, trial and error, etc. Unfortunately, the weight window generator can produce both good and bad results, forcing the user to decide if the results are reasonable.

The weight window technique was applied to the high altitude problem to see if the technique was not only feasible but helpful. Several problems arose when implementing this technique. Initial guesses of the space-energy parameters were input according to suggestions in reference 7. The output information provided by the weight window generator was mostly useless, providing no improved information on the space-energy cut-offs. After several more tries with this technique, it was abandoned in favor of using only geometric splitting/Russian roulette.

3.6 MCNP Tallies And Detectors

MCNP provides several standard types of tallies, six types for neutrons and five types for photons; each tally is normalized "per starting source particle". Descriptions of each of these tallies are provided in the MCNP manual, chapter 2, page 80. Because no results were obtained for the low altitude problem, the tallies and detectors used in the high altitude problem will be discussed. Table 2 lists the tallies used in the high altitude problem and the corresponding tally/detector descriptions and units as given on page 82 of the MCNP manual.

Table 2
MCNP Tallies

Tally	Units	Description
F2	$1/cm^2$	Surface Flux
F4	$1/cm^2$	Track length estimate of cell flux
F5Z	$1/cm^2$	Flux at a point (ring detector)
*F4	MeV/cm^2	Track length estimate of cell energy flux
*F5Z	MeV/cm^2	Energy flux at a point (ring detector)

No user modifications to these tallies were made, even though this is allowed in MCNP. The above tallies were used to give the average flux across the cell surface, the track length estimate of flux averaged over a cell (volume tally), and flux at points located on a ring through a cell.

The units of the F2 flux tally are the units of the source, explained in Section 4.2.1 of this report. In this case, the source units are in terms of fraction of particles within the source spectrum energy bin per source particle. Thus, since there is no time dependence to this problem, this tally is really a fluence tally. (In the remainder of this discussion, "flux" is used to conform with the MCNP documentation, but "fluence" is meant.) This tally then gives a surface flux estimate which is averaged over a specific surface bounding a cell.

The units of the F4 tally are identical to those of the F2 tally, and are defined in the same way as the F2 tally. The difference in using this tally is that it gives you a track length estimate of the flux averaged over a cell instead of just a specific surface. It is important to maintain a constant cell population from cell to cell. The F4 tally becomes important when comparing ring detector values at cell center or at some other point within a cell to the average value over a cell. These two tallies will tend to differ depending on the source to detector distance and the optical thickness of each cell.

The units of the ring detector tally are identical to those of the other two tallies. A ring detector is useful when the user is interested in the average flux at a point on a ring about a coordinate axis, in this case the vertical or z-axis. Ring detectors were employed to enhance the efficiency of point detectors because of the low probability of a particle contributing to the dose to a detector at a large distance

from the source. Azimuthal symmetry was assumed in defining the problem, which lead to the use of a cylindrical coordinate system, an ideal case for ring detectors.

For the high altitude problem, ring detectors were employed not only to compare cell average fluxes with point values within a cell, but also to compare the errors versus run times for both tally types.

The units of the *F4 energy tally differ from those of the F4 tally in that the *F4 tally is an integral of the energy deposited from each particle in the cell. It is used in the same way as other tallies.

The units of the *F5Z detector tally are identical to those of the *F4 tally. The *F5Z detector becomes useful when the user requires the average energy flux at a point on a ring about a coordinate axis, in this case the z-axis. The same advantages and disadvantages inherent in using ring detectors hold for ring energy detectors as well.

4 Details of the Test Cases

4.1 Point Source at High Altitude

4.1.1 Geometry Description

As discussed previously, mass-integral scaling is known to work poorly at high altitudes, therefore a Monte Carlo simulation of transport from a high altitude point source was assumed to be able to provide a better answer but at an unknown computational cost, presumed to be high. The first step in setting up a Monte Carlo simulation is to divide up the region of interest into an "adequate" geometry to obtain answers with good statistical errors. Several constraints drive the selection of such a geometry for an atmospheric transport simulation, the most important of which is the variable density of the atmosphere with height. This presents a complication for most Monte Carlo codes which are set up to deal with homogeneous media. This density gradient demands a geometry which is split up into vertical slices; the azimuthal symmetry of the problem makes cylindrical slices a natural coordinate system to use. Another factor which drives the selection of a problem geometry is the variance reduction requirement. The most straightforward variance reduction technique is geometric splitting at cell boundaries; one needs to provide enough cell boundaries so that one can generate cell importance factors such that a roughly equal number of neutrons enter each cell. A third geometry issue specific to this study was the plan for a possible future comparison of the Monte Carlo results with a discrete ordinates calculation of the identical

problem. Ideally one would calculate the same problem on the same geometric mesh with both Monte Carlo and discrete ordinates and obtain a direct comparison of the two approaches.

All these factors would lead one to generate a fine geometric mesh with a large number of cells. However, as the number of cells is increased, the computational cost will increase, nonlinearly with the use of geometric splitting. In order to keep the run times less than a few days, and because of the time-consuming processes involved with the input of large numbers of cells and analysis of excessive volumes of output, we choose to limit the spatial mesh to no more than 200 cells. Working within this constraint, the mesh shown in figure 2 was developed for the high altitude simulation. At each height, the distance for the vertical spacing was selected to be approximately one mean free path for a two MeV neutron, since two MeV was the average energy of the source spectrum used. At a height of 20 km, this mean free path is roughly 1 km. The exponential scale height of the atmosphere is approximately 7 km; the half scale height, the distance over which the density changes by a factor of two, is about 5 km and is a more useful number. For the majority of cells in the problem the density changes by a factor of two from bottom to top. The uniform density used for the cell for the Monte Carlo simulation is the calculated average density across the height of the cell, so that the total mass contained in a vertical slice of the atmosphere is conserved.

Above 100 km, the mixing ratios were obtained from the US Standard Atmosphere (Appendix C). Instead of using an exponential density profile, the values from the US Standard Atmosphere were integrated and this average value used. The regions above 100 km were shown to be unimportant for a 40 km source altitude. A comparison of two runs, one having a vacuum boundary at 100 km, and one including the regions above 100 km showed no statistically significant differences. Examination of the MCNP output file showed that while the same number of neutrons entered all cells in the problem, no collisions occurred in these regions because the atom density is so low.

This last fact is the key reason why the MCNP simulations for a high altitude source were successful: this is an optically thin problem! While a co-altitude distance of 100 km may seem to be very large, for a 40 km source height, this is only 4 or 5 mean free paths. In this high altitude problem (unlike the low altitude simulation) neutrons reached every region of the problem without any variance reduction, so tweaking the cell importances to transport equal numbers of neutrons to all regions of the problems only required one or two MCNP runs.

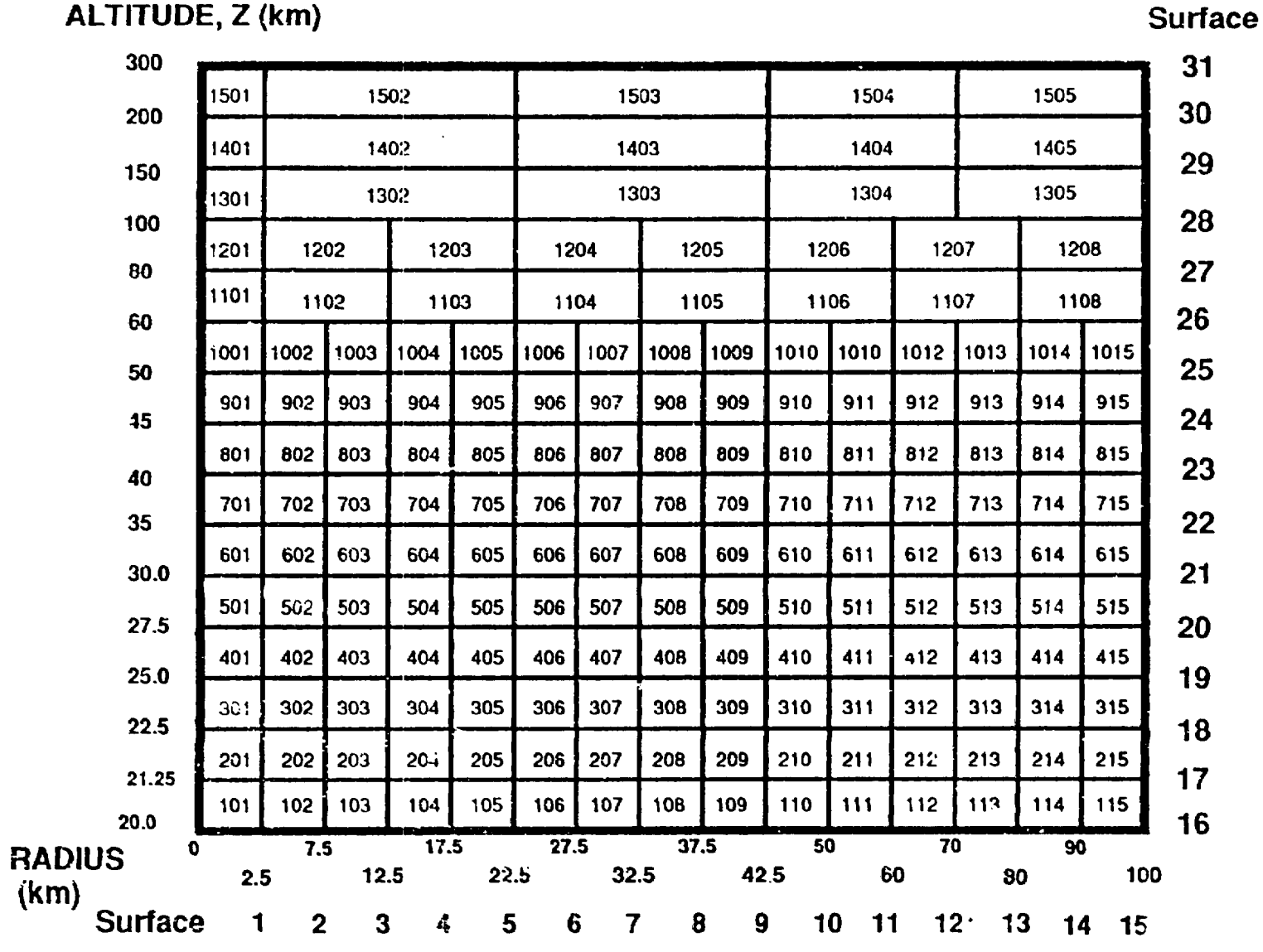

FIGURE 2 Spatial cells for the High Altitude Case

The cell structure used for the 40 km source altitude simulation is shown in figure 2. The vertical dimension is divided by planes perpendicular to the z axis. The horizontal dimension is divided by cylinders parallel to the z axis. The heights of the planes and the radii of the cylinders are listed. Also listed is the number of each surface as used in the geometry specification of the input file. For example, in MCNP one defines the volume of Cell 505 as being ABOVE Surface 20 (+20), a plane perpendicular to the z axis at a height of 27.5 km, BELOW Surface 21 (-21), a plane perpendicular to the z axis at a height of 30.0 km, OUTSIDE Surface 5 (+5), a cylinder concentric to the z axis with a radius of 22.5 km, and INSIDE Surface 6 (-6), a cylinder concentric to the z axis, with a greater radius.

The outside of the problem is modelled as vacuum. This is not a realistic boundary condition, so the neutron fluence in the outermost cells was never calculated. An earlier geometry only had a radius of 42.5 kilometers; a comparison of the results from the earlier geometry versus that of figure 2 showed statistically significant differences only in the outer cells. An alternative approach is to use reflective boundaries with some albedo estimated using MCNP to compare the fluences of the outermost cells and those in the next layer in; however, it is more reliable to neglect the outermost cells.

Although the atmospheric density variation with altitude and azimuthal symmetry inherent in this problem make cylindrical geometry convenient for a high altitude point source, there is an alternative geometry which seems natural. If the atmosphere were homogeneous, one would expect constant fluence along surfaces of constant range, i.e. spherical symmetry. The atmospheric density gradient skews these surfaces, making them closer in going down into thicker air and farther apart going up into thinner air. These surfaces of constant optical thickness are shown in figure 3, in units of τ_∞, which is the optical path length that a neutron would see going straight up from the given altitude to infinity, i.e., at a source elevation angle of +90 degrees. τ_∞ at a source height of 40 km is an optical thickness of 0.292. However, as seen in figure 3, these surfaces are not closed for τ greater than τ_∞. Physically, this means that above a certain elevation angle, there is not enough air along that direction to provide that large an optical path length before the neutron escapes. Notice that for negative source elevation angles, i.e. below the source point, the surfaces are always defined. These surfaces are interesting because they are the surfaces which have constant mass integrals, and one would expect SMAUG-II to provide results governed only by spherical divergence along them.

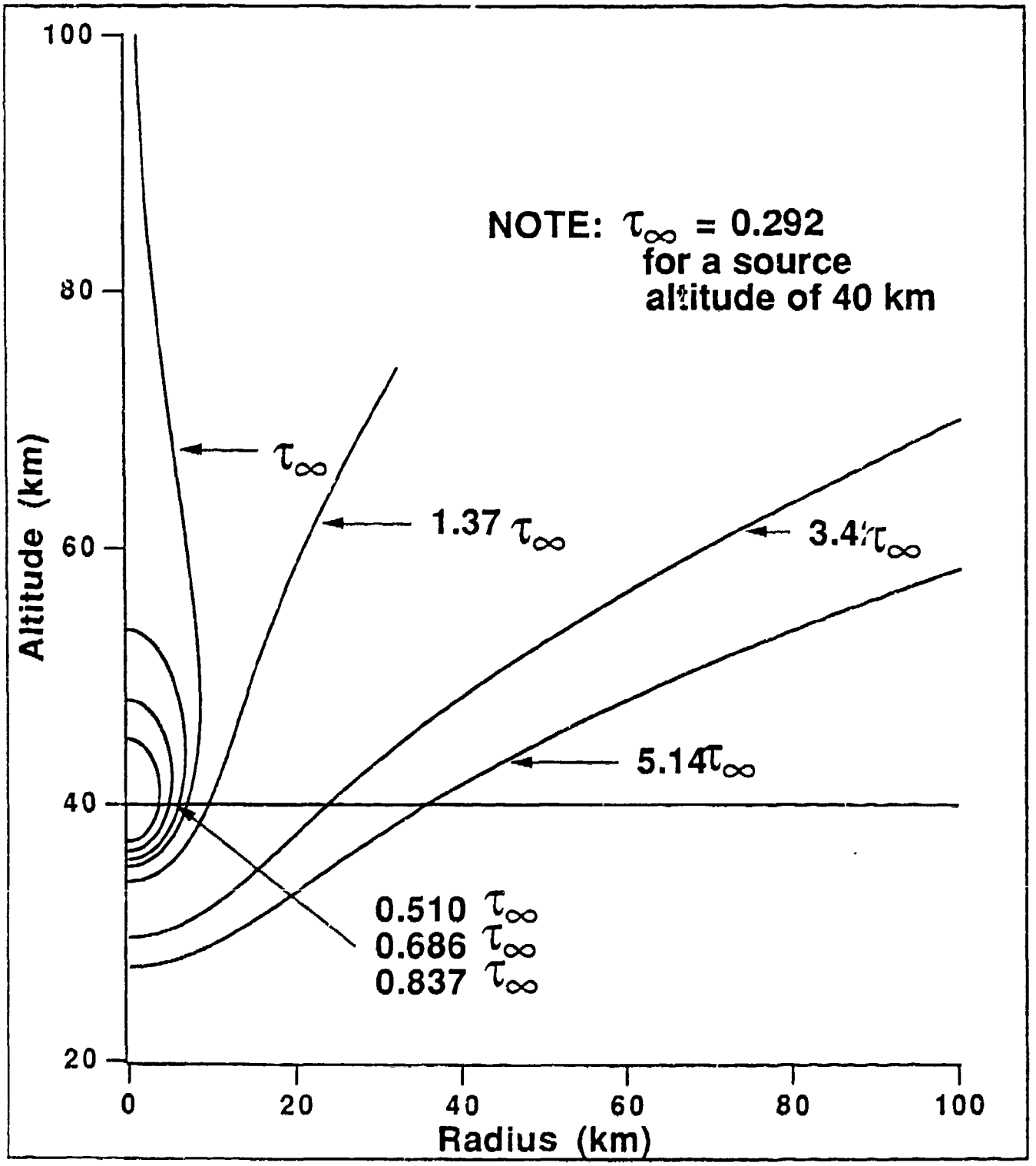

FIGURE 3 Contours of constant optical thickness.

4.1.2 Problem Discussion

After this mesh was developed, the following procedure was used to calculate the cell importance for geometric splitting. An MCNP calculation with 50,000 source neutron tracks with all cell importances equal to 1.0 but without any detectors was run. The output file from MCNP lists the neutron tracks entering and population in each cell. A cell importance of 1.0 was assigned to the cell containing the source point, and the importances of the other cells was calculated to normalize the tracks entering each to the number in the source cell. The problem was then rerun with the new cell importances, and the tracks entering each cell checked. Except for an occasional typo (the cell importances were entered manually), the tracks entering each cell would be constant to 2% to 5% after one iteration. A similar procedure was attempted for photons once, but was not as successful. This can be attributed to the fact that only n-gamma reactions were included in the calculations, i.e., no photons from the source. The gamma creation source is distributed throughout the problem mesh, and splitting only affects those secondary photons which cross boundaries. Geometric splitting may not be the best method to optimize the gamma population. Time constraints prevented a more thorough investigation of the neutron induced photons in this problem.

The selection of detectors evolved during an initial phase of test problems in homogeneous, low density (30 km equivalent) air. Our first detector was a 10 meter diameter Al sphere located at a range of 7 km from the source point. However, unless this sphere is centered on the z-axis, the cylindrical symmetry of the problem is broken and MCNP will not calculate the volumes of all the regions correctly. For a quick fix, the sphere was moved to a point on the z-axis, 7 km directly above the source point. With no variance reduction, source biasing, etc., no collisions with this sphere were recorded for a run with 10,000 source neutrons. The sphere was moved to a point 1 km above the source and we still could not hit it! This very quickly demonstrated an inherent limitation of Monte Carlo; it does not give good results for small regions. While a 10 m diameter sphere doesn't seem like a small radiation detector, it is very small in terms of the solid angle subtended, even at 1 km.

There are techniques which could have been employed to try to overcome this problem, though not without a proportional computational cost. These techniques have been discussed previously in this report, and are well described in the MCNP manual. Based on these results, instead of trying to use "detector volumes", it was decided to use two of the tallies built into MCNP; cell average tallies for mapping purposes, and ring detectors for point answers. Cell average tallies for the cells used in this problem are only useful for mapping because the cell volumes are so large, i. e., the cell average is not the value

at the cell center. For cells close to the point source, where the gradients are large, the cell average is of limited value even for this purpose. A comparison of the cell average fluence and the cell center fluence determined from ring detectors showed the difference was as large as a factor of 5 in cells two layers away from the source, and around a factor of 2 different farther away from the source. Ring detectors with a radius of 100 m were also used to provide point answers which could be directly compared to SMAUG which provides point answers. Because ring detectors calculate the effect of every particle run in the problem, they are computationally expensive compared to cell average tallies. While MCNP will calculate up to 100 cell average tallies per run, one is limited to only 20 ring detectors per run. The combination of high computational cost and limited number of detectors makes it impractical to map out the fluence using ring detectors. Instead, the ring detectors were placed on surfaces which would highlight the differences between mass-integral scaling and the Monte Carlo results: surfaces of constant range (spherical shells), which would show a response independent of source elevation angle in a uniform atmosphere, and surfaces of constant optical path length, on which one would expect to see a response proportional to the inverse square of the range due to spherical divergence.

4.2 Point Source at Low Altitude

4.2.1 Geometry Description

The primary goal in determining the geometry for a particular problem is to model, as accurately as possible, the geometric features and the material properties that are inherent in the problem definition. A secondary goal is to obtain the simplest geometry possible without overly compromising its validity. By retaining certain symmetries in the problem, the complexity and computation time can be reduced. The only geometric feature inherent in the low altitude problem is the airspace itself, which is, for all practical purposes, unbounded relative to low altitudes. The primary material feature to keep in mind is the changing atmospheric density with altitude. The density values over several tens of kilometers vary by a few orders of magnitude, and can drastically affect the transport characteristics of the neutrons and photons. The goal then, is to "contain" the surrounding airspace within certain geometrical limits while recognizing the need for variation of density at certain altitudes or "bands" of altitudes.

The final geometry used for both the high and low altitude problems was a result of previous investigations into the best methods for modeling the airspace surrounding the point source. To scope the problem, we first used concentric spheres centered around the source. This simple geometry allowed us to not only become

familiar with running MCNP, but allowed for a few simple analytical results to be calculated as benchmarks for MCNP results. It became apparent that a cylindrical geometry would be best in that it would be simple to implement, simple to visualize, and would allow for modeling the problem more accurately by introducing variable atmospheric densities.

Advantages to this geometry include simplicity and function; the geometry is simple to visualize by an unfamiliar user. This geometry is also relatively easy to input into the MCNP input file, "INP". To take advantage of the assumed azimuthal (or rotational) symmetry, cylinders of increasing radius were used to define the vertical surfaces. The horizontal surfaces were defined by planes of increasing altitude. The MCNP input file "INP" for this problem is given in Appendix A, where the cell and surface specification cards are listed first. Each major portion of the "INP" file is explained in order to aid the unfamiliar user in comprehending the geometry. The graphical representation of the geometry used in the low altitude problem is shown in figure 4.

As seen in figure 4, only the right half of the cylinder is shown, since the problem is assumed to have azimuthal symmetry. The problem is thus modeled in three dimensions with the restriction that rotational symmetry be employed. The size of the problem is limited in that there is only 15 kilometers of horizontal distance and 20 kilometers of vertical distance. The vertical distance exceeds the horizontal distance to reduce the leakage rate of particles out of the top surface. This is due to the reduced density of air at higher altitudes. There are 179 cells defined in this geometry. Each cell is bounded by cylindrical surfaces on the left and right and by plane surfaces on the top and bottom. Each cell and surface is defined separately in the "INP" file (see Appendix A), and each is referred to by a separate cell or surface number. In this case, surface numbering begins with the innermost cylinder (surface 1), progresses outward until the outermost cylinder is reached (surface 10), and then begins at ground level (surface 11) and progresses upward until the top-most surface is reached (surface 31).

The cell structure shown in figure 4 was chosen based primarily on a 200 cell limit. The cell numbering scheme was chosen to resemble the indexing of a matrix, allowing easier identification of cell locations within the geometry. Because of the 200 cell limit, the sizes of each cell were large relative to the mean free paths of the neutrons. At sea level (0 kilometers), the total mean free path (scatter + absorption) of a neutron is approximately 120 meters (table 1). The absorption mean free path of a neutron is much farther, but analysis of the cross sections showed that particle transport

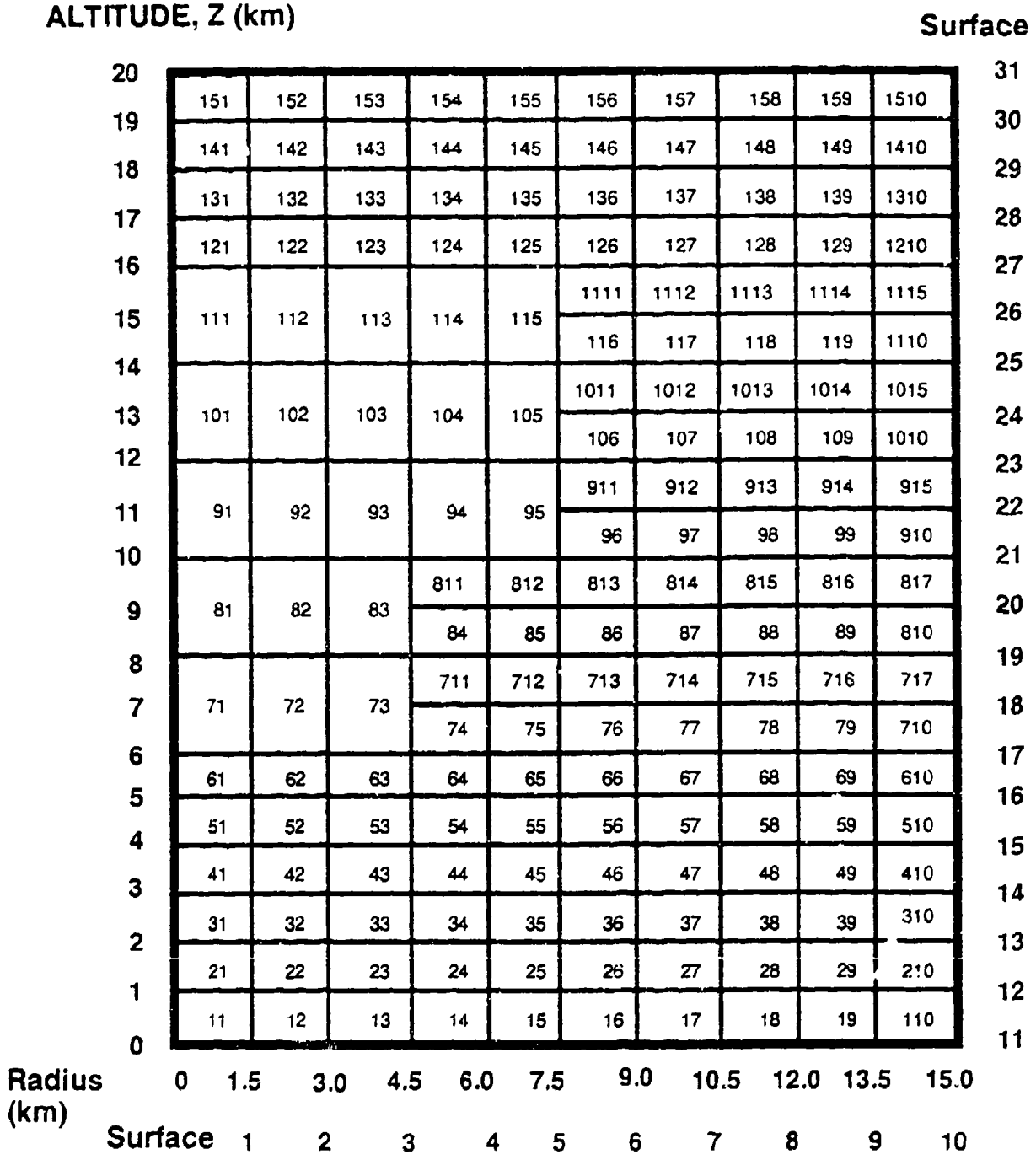

FIGURE 4 Spatial Cell For Low Altitude Case

is dominated by scattering in air. Therefore, at sea level, each cell is approximately 12 mean free paths in thickness, a serious problem when trying to transport a sufficient number of particles over several kilometers. This invariably means that high importance values are required at each cell boundary, and will increase with increasing distance from the source.

For simplicity, the source was modeled as an isotropic point source, located at an altitude of 11 kilometers, and in the center of cell 91. It is not recommended that a source be placed on a boundary; this could lead to problems in determining the true importance weighting between cells. The cell sizes in the immediate proximity to the source were expanded because transport of the particles was not a problem at these distances. This conserved the number of cells use in the problem while decreasing the overhead required in implementing the geometry, the importances, etc. At distances farther from the source, the cell sizes were smaller and remained constant throughout the rest of the problem to aid in particle transport.

4.2.2 Problem Discussion

The primary goals in the analysis of the low altitude problem were to examine the free-field fluence and dose from a point source at a specified altitude within the atmosphere and to provide results for comparison against SMAUG II. The source was taken to be an isotropic point source for simplicity. The source spectrum used is described in Section 3.2.1 and can be found in the source specification cards within the "INP" file given in Appendix A.

The first step in the analysis of this problem was to determine the best geometry. It was determined that a cylindrical geometry is naturally suited for a problem of this type so that variations in atmospheric density could be implemented easily without undue complexity in the geometry. The source was placed at an altitude of 10 kilometers for earlier runs and was changed to 11 kilometers in later versions of the geometry.

At first, only simple geometries such as spheres and cylinders with no internal structure (cells) were used, in order to become familiar with running MCNP and determining the major transport characteristics of the neutrons and photons. Several factors became apparent during this early analysis, and are listed as follows:

1. scattering is the dominant transport mechanism for both neutrons and photons,

2. absorption is present, but is a minor characteristic except at low energies, where the absorption cross-section becomes larger,

3. the average energy of the neutrons is approximately 1.98 MeV,

4. mean free path for neutrons at very low altitudes is approximately 120 meters, and increases with increasing altitude, and

5. the contribution due to nitrogen scatter is a factor of nine greater than the contribution due to oxygen scatter, even though the difference in weight percentage is roughly a factor of four.

As the amount of information pertaining to the particle transport characteristics increased, it became clear that no particles were reaching the outer boundaries of the cylinder, primarily because the particle weights were so small that they were Russian rouletted long before reaching the outer boundary. It was necessary to gradually increase the complexity of the geometry by increasing the number of cells in order to provide splitting surfaces for geometric splitting/Russian roulette. The importance factors for each cell had to be obtained by turning off all tallies and detectors and running a few thousand particles so that new importance factors could be calculated.

At this point, still no success was achieved in transporting particles more than a few cells away from the source. The next step was to increase the number of cells to an already growing number of cells within the geometry. Particle transport still proved to be extremely difficult at distances greater than three or four cells away from the source cell. The vast majority of particle tracks ended primarily through Russian roulette due to low weights. It was decided that increasing the number of cells up to the limit of 200 cells was necessary. A 200 cell working limit had been chosen so an excessive amount of user overhead and run time could be avoided. At this point, 179 cells had been defined. This greatly increased the manhours necessary to redefine the geometry and run test cases to determine importances. The initial importance factors that had been input as guesses proved to be too small for adequate particle transport, so the importance factors were increased by an order of magnitude and the run repeated. By this time, importance factor guesses ranged from a value of 1 at the source to 5000 at the outer cell locations relative to the source. Problems with computer failure of the ELXSI computer at AFIT became a major source of aggravation and work

stoppage. The mean time between failure of the ELXSI became less than the run time for the geometric splitting/Russian roulette alone, with no tallies or detectors. For the reasons described above, the latter geometry configuration never ran to completion, even after seven restarts. The actual run time for splitting alone is currently unknown. The longest run time attained thus far was 2600 minutes of live cpu time, where the cpu usage varied between 25 and 50 percent, implying that the real time would be at least twice 2600 minutes for job completion.

The latest geometric configuration used is shown in figure 4. The cell and surface card specifications for this geometry are shown in Appendix A. The importance values shown are not necessarily the correct values, but merely guesses, and give the user an idea as to the magnitude of the splitting ratios required to reach the outer cells.

Based on the above analysis and personal experience, the Monte Carlo technique at low altitudes is impractical because of long run times, high importance factors, and limitations imposed by the large number of cells required to achieve adequate particle transport.

5 Comparison of Results

5.1 High Altitude Simulation

5.1.1 Cell Average Results

The results of the MCNP calculations using cell average tallies for cells closest to co-altitude and above are shown plotted against horizontal radius ("ground range") in figure 5. The tally plotted is the energy deposited in the cell in MeV per gram per source neutron. MCNP provides the option to calculate either cell average neutron fluence or energy deposited, and because the ultimate goal of these simulations is dose prediction, the energy option was selected. Because of time constraints we were unable to convert these results to rads silicon or rads tissue.

The location of the cell average tally is plotted as though it occurred at the cell center. Plotting these results as a function of height and radius makes them easy to visualize using the geometry shown in figure 6. (The numerical values of the results from the 40.05 km source altitude radiation transport simulations are listed in the table in Appendix B.) The curve labeled at a height of 47.5 km corresponds to the cells 01 to 14 in row 9, which have a center height of 47.5 km. The curve at 42.5 km is made up of the co-altitude cells, etc. It is more informative to plot these results against range, as is

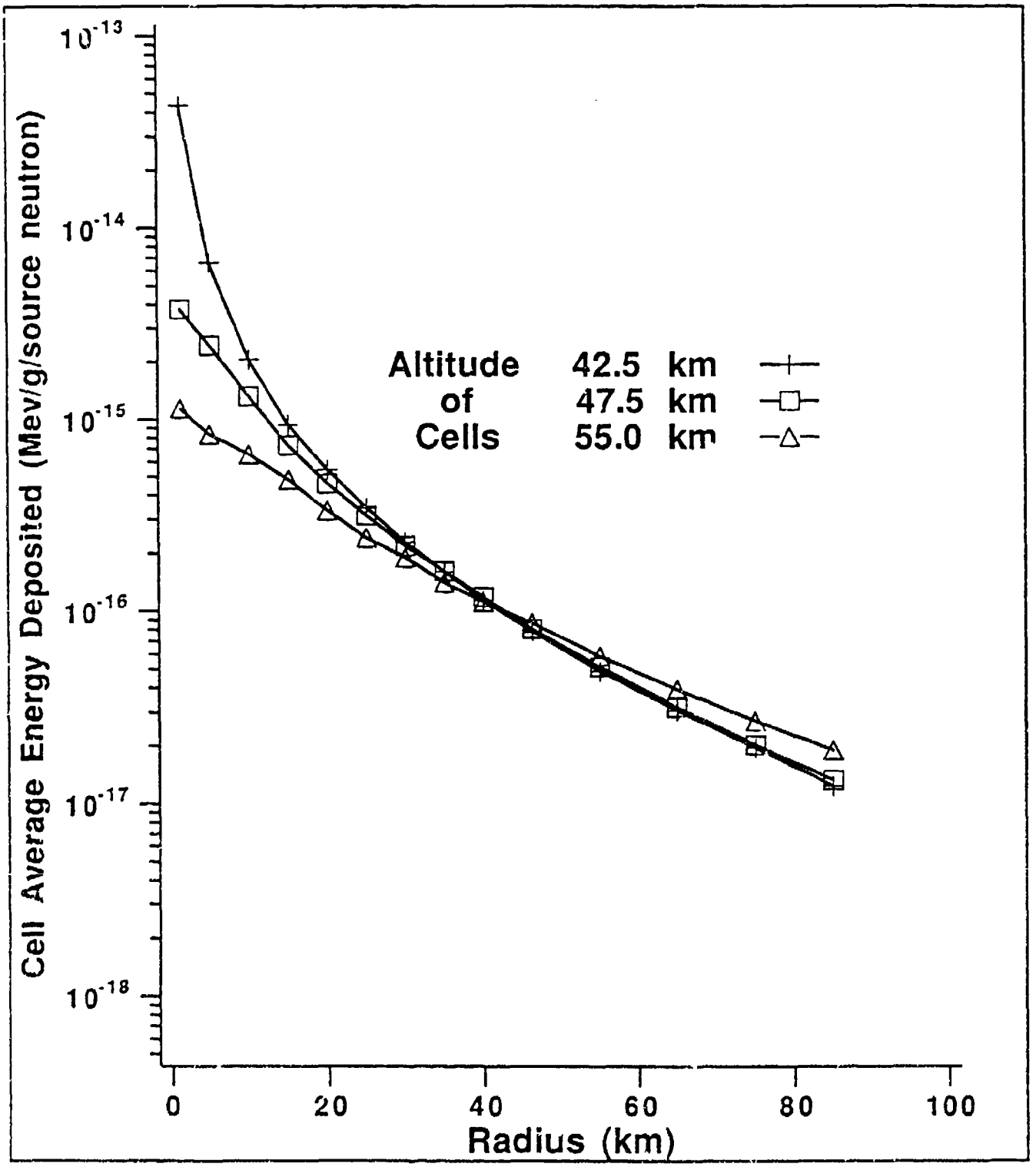

FIGURE 5 Average neutron energy deposited in a cell for cells co-altitude and above the source as a function of radius

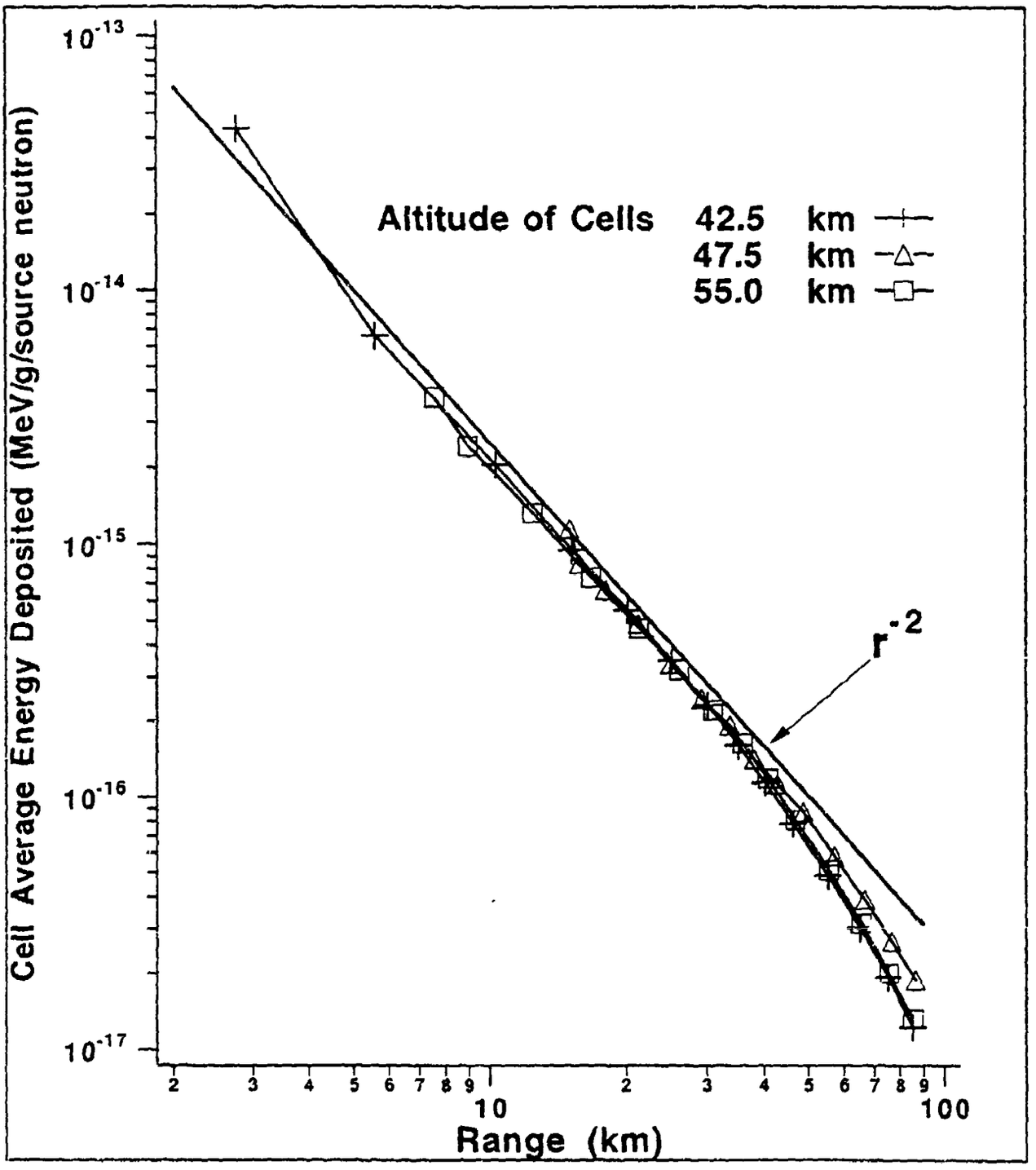

FIGURE 6 Average neutron energy deposited in a cell for cells co-altitude and above as a function of range

done in figure 6. On a log-log plot, a curve which has a power dependence appears as a straight line with a slope equal to that power. An r^{-2} curve is plotted for reference on figure 6, which is the prediction of spherical divergence. As is seen, the energy deposited follows the spherical divergence prediction out to approximately 40 km, and then begins to decrease faster than r^{-2}. This occurs because at ranges greater than 40 km above the source point, attenuation by the atmosphere begins to dominate. The result at a range of 3 km is significantly higher than the spherical divergence prediction because this is the cell average tally for the cell (cell 801 from figure 2) which contains the point source. The gradient across this cell is large, so the cell average does not accurately represent the value at the cell center.

The cell average energy deposited for cells closest to co-altitude and below the source point is shown in figure 7, plotted as a function of radius ("ground range"). Figure 8 shows these same results plotted as a function of range ("slant range"). As before, the cell average shows deviation from r^{-2} relation closest to the source because of the large gradients present in the cells closest to the point source (cell 801 and 701 in figure 2). Again the results show the dominance of spherical divergence close to the source, but because the path to these cells from the source is down into thicker air, the faster than r^{-2} falloff of the energy deposited caused by attenuation begins to show up at 20 km, one-half the range as was seen for cells above the source. The greatest deviation from the r^{-2} behavior is seen for cells which are lowest below the source (22 km height corresponds to the cells in row 2 of figure 2) which have the largest mass integral, hence the largest attenuation. As seen in figure 8, this behavior occurs monotonically as the cell locations go down into thicker air, as one would expect.

MCNP provides a statistical error estimator which is the reduced standard error of the mean. Table 2-3 of the MCNP manual gives guidance for the confidence level of the answer based on this estimator. The errors for the cell average tallies were for the most part 0.05 or less, with one or two cells which were "hard to hit" because of the problem geometry having errors around 0.10. The confidence of these results based on this error estimate is good. The errors are not plotted on any of the figures because they are smaller than the symbol markers on the logarithmic scale, however, they are listed in Appendix B.

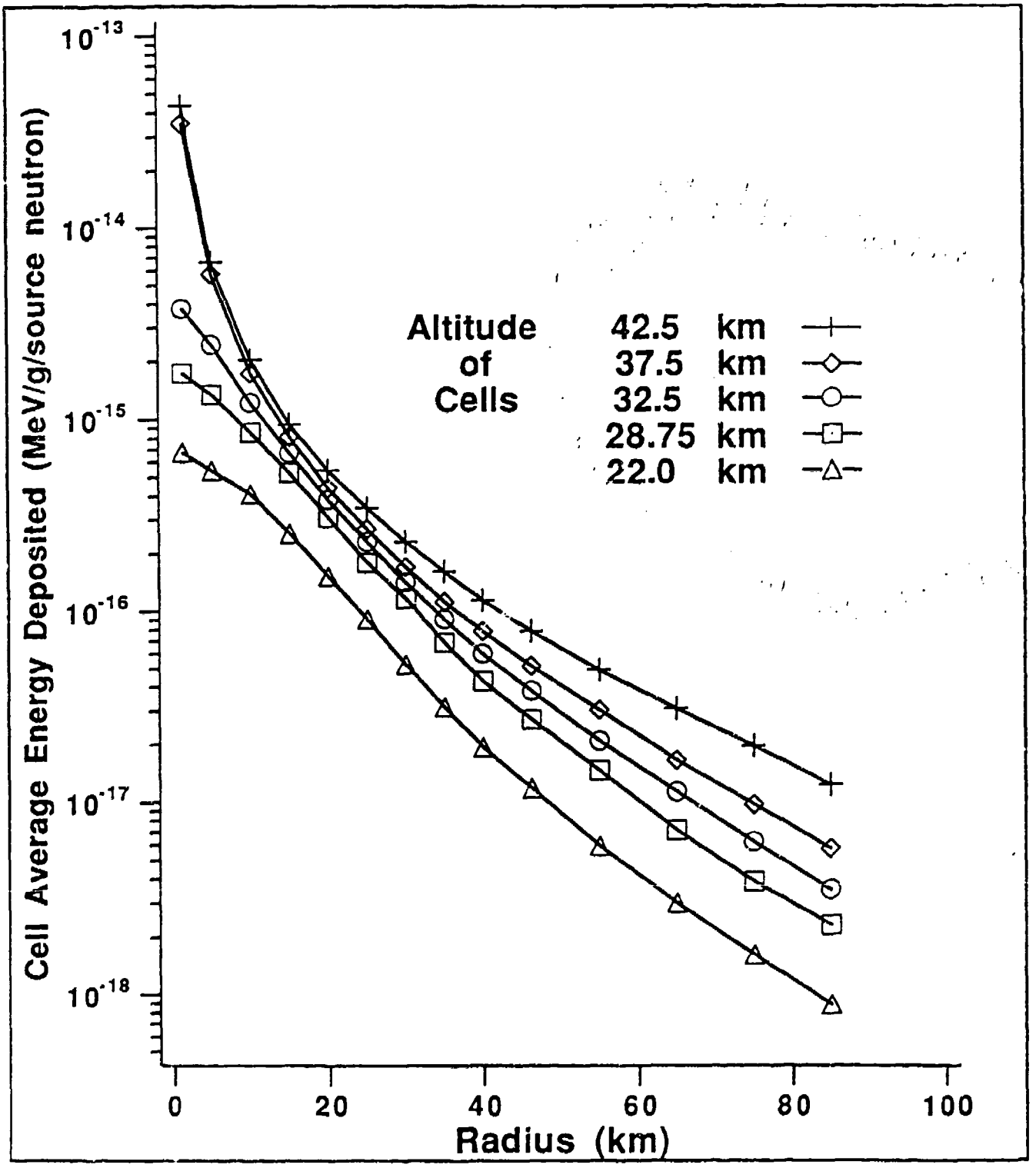

FIGURE 7 Average neutron energy deposited in a cell for cells co_altitude and below the source as a function of radius

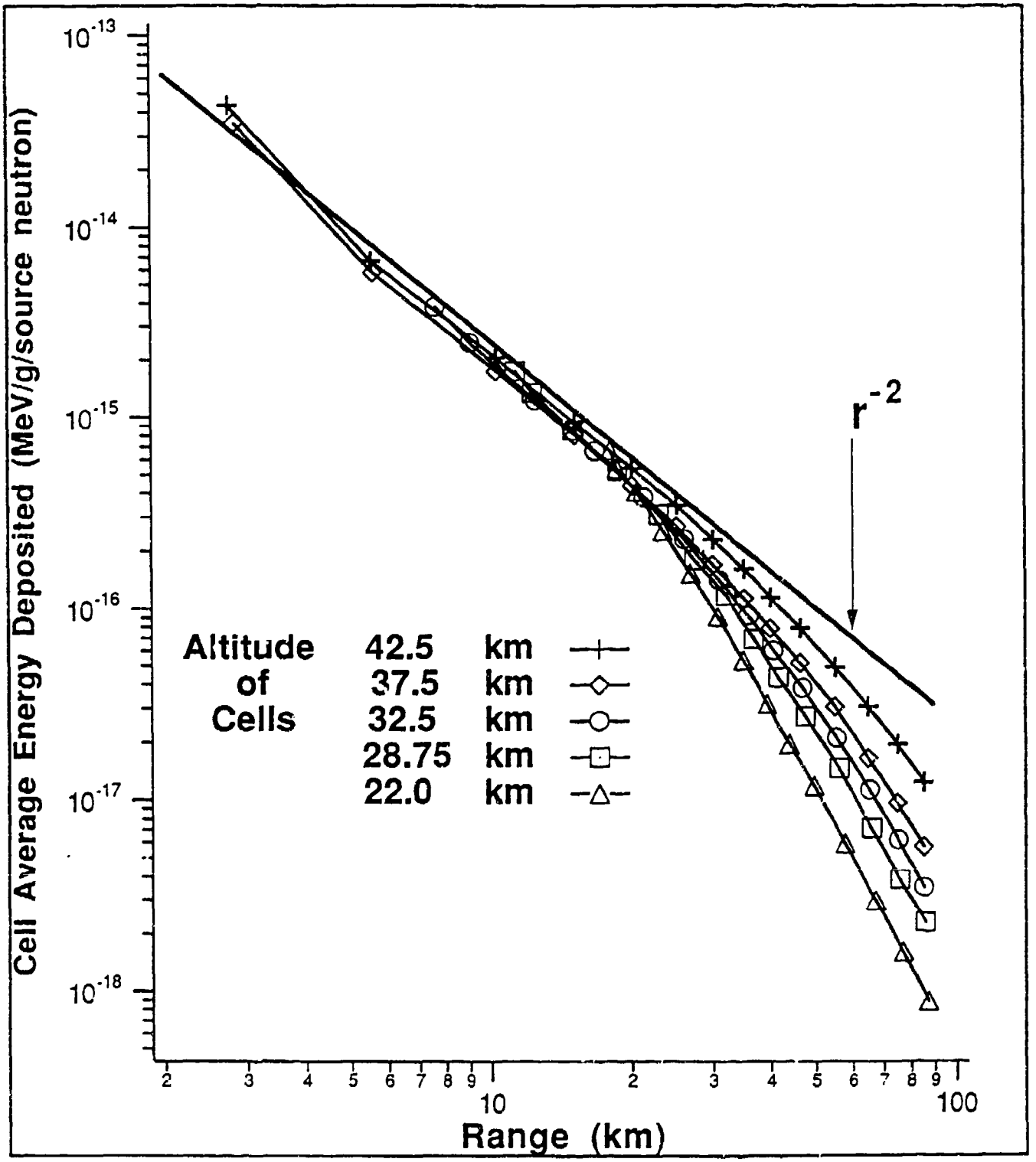

FIGURE 8 Average neutron energy deposited in a cell for cells co-altitude and below the source as a function of range.

5.1.2 Ring Detector Results

The results from the cell average tallies display reasonable behavior and demonstrate that the geometry selected for the problem is "good", but "good" cannot be quantitatively defined because these results cannot be directly compared to any other references. As was mentioned earlier, the cell average tallies are not computationally expensive; for the results discussed a total of 98 cell average tallies per run were calculated. For comparison to the mass-integral scaling (MIS) results produced by the computer code SMAUG, point answers are required. Because it is extremely difficult to hit small detector volumes with the Monte Carlo method, the ring detectors built into MCNP were used to provide point answers. (A point in an azimuthally symmetric geometry maps into a ring.) Because the ring detectors were built into MCNP, use of the ring detectors did not require the problem geometry to be specifically tailored to obtain transport with good statistics to one or two locations. Modification of the input file to obtain an answer at a specific ring location is a trivial two line change. However, reinforcing the observation that the product of speed and usefulness is a constant, ring detectors proved to be computationally expensive (computational costs will be compared later in this section). In MCNP, ring and point detectors can only provide the fluence, not the energy deposited. Information on the spectrum can be obtained from other features of the code, however, comparisons with SMAUG were performed with the fluence results because this was simpler.

Figure 9 shows the results from MCNP calculations of fluence per source neutron on surfaces of constant range at source elevation angles from +90 degrees (directly above the source point) to -90 degrees (directly below the source point). At a range of 3 km, the fluence is fairly constant over all angles because the range is small compared to the scale of variation of the atmospheric density. For ranges from 6 to 12 km, the fluence increases as one scans through the angles from above to below the source. This result is explained by the fact that neutron flux or fluence is greater in regions where there are more collisions because the neutron track length is greater. The increasing density with decreasing altitude means that each neutron will experience more collisions below the source and contribute more to the fluence, i.e., one observes buildup from scattering. Above the source, each neutron undergoes fewer collisions so the fluence per neutron is smaller, i.e., above the source one observes streaming behavior. At ranges of 15 and 18 km, the fluence increases with decreasing source elevation angle, but reaches a maximum and then decreases.

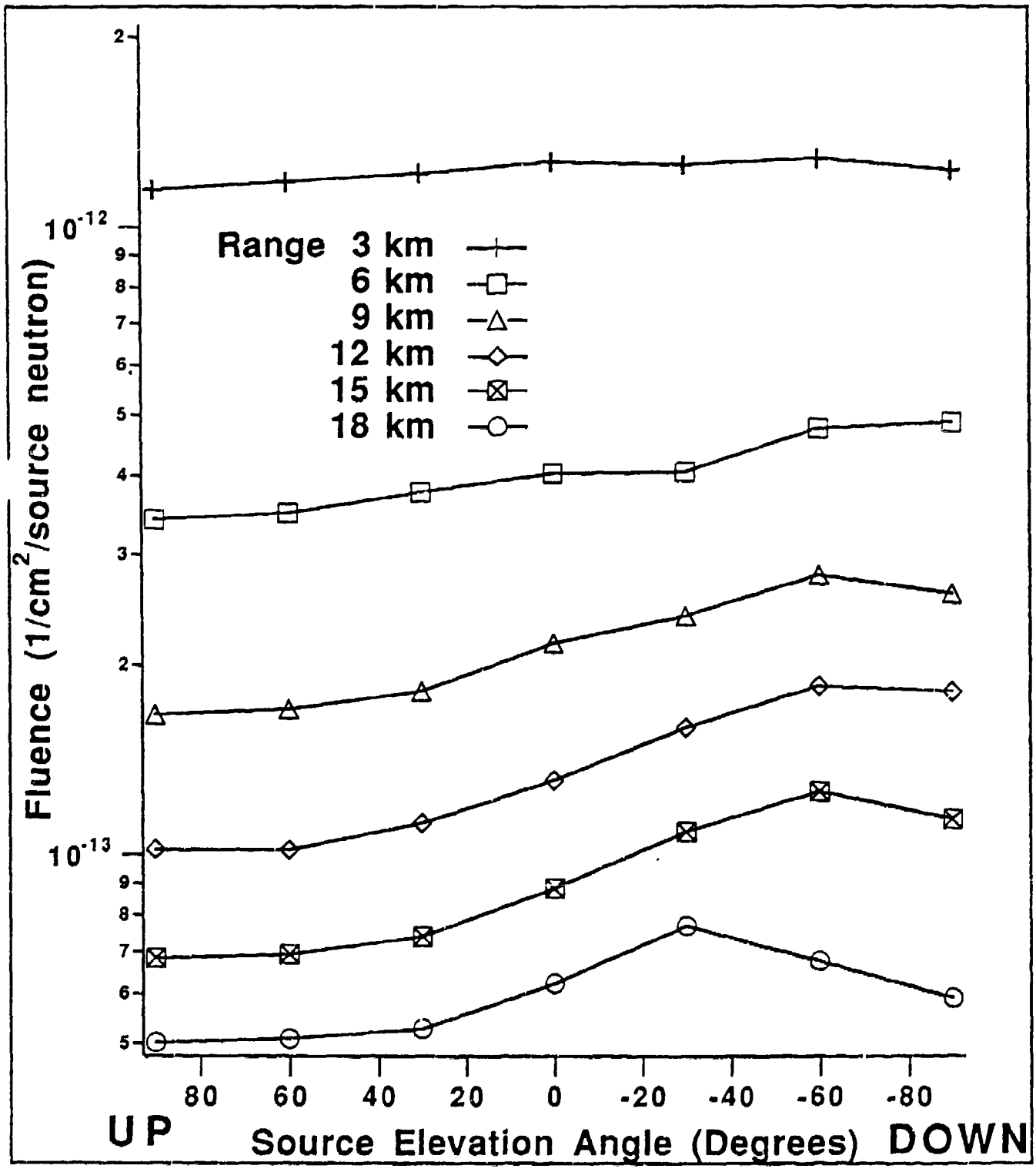

FIGURE 9 Neutron fluence calculated by MCNP using ring detectors on surfaces of constant range as a function of source elevation angle.

These paths at the largest range and the most negative source elevation angles have the largest mass integral, and attenuation begins to dominate over buildup from scattering.

Figure 10 shows the SMAUG results for the same detector locations as shown in figure 9 on the surfaces of constant range. The same trends are observed in the SMAUG results as in the MCNP results: small variation at the closest range, buildup from scattering in thicker air below the source at intermediate ranges, and eventually attenuation dominating buildup at the largest mass integrals. However, the SMAUG results are consistently higher in most regions of the problem than the MCNP results. A comparison of these results is shown in figure 11, where the values of $100\times(SMAUG-MCNP)/MCNP$ are listed. The behavior seen here is best explained by neutrons emitted in the downward direction being scattered up and escaping, a mechanism which is not accounted for by MIS. It appears that in this comparison the total number of neutrons is not conserved, i.e., SMAUG is lower below the source point more than MCNP is higher above it. This occurs because the fluence is dependent upon the collision density; those neutrons which scatter up escape with fewer collisions and contribute less to the fluence than neutrons below the source.

The errors of the ring detectors at these locations were almost all less than 0.05, with the exception of the results for the ring detectors directly below the point source at ranges of 15 and 18 km, which had errors of 0.08 and 0.10. The error tolerance on the results of ring detectors is more stringent than for cell average tallies, however, these error levels indicate these results have good confidence.

For another comparison between SMAUG and MCNP, ring detectors were placed on surfaces of constant optical path length at source elevation angles from +90 degrees to -90 degrees for specific values of τ less than τ_∞ at 40 km. Since the surfaces of constant optical path length become undefined for source elevation angles greater than a critical angle for τ greater than τ_∞, positive elevation angles could not range up to 90 degrees. Figure 12 shows the results of the MCNP calculations. The same basic trend is observed again as in the results for the constant range cases: the flux increases downwards into thicker air. The flux does not decrease at the lower elevation angles because the attenuation on the surfaces of constant optical path-length is equal. Figure 13 shows the SMAUG results for the same detector locations. Again the same trends

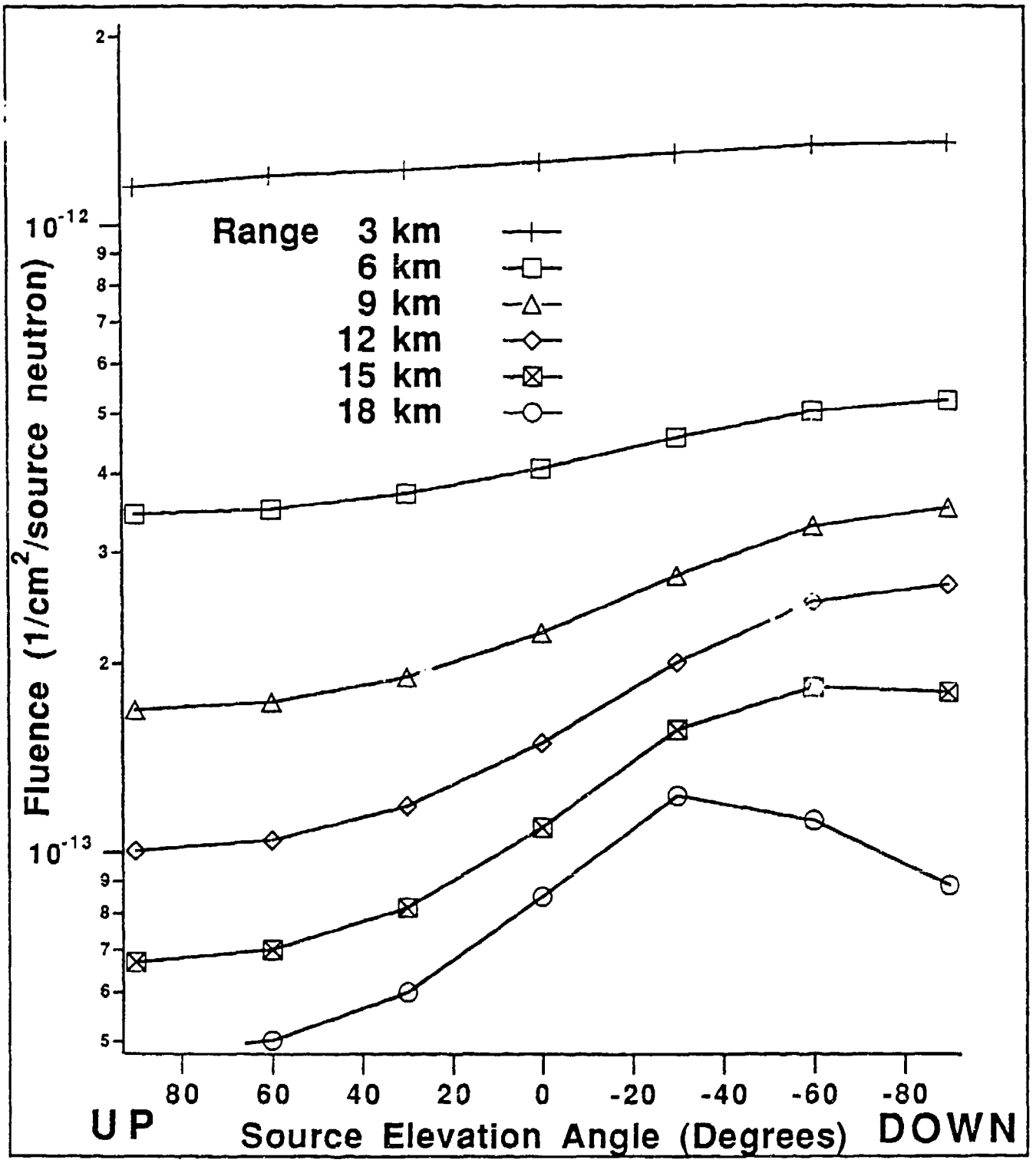

FIGURE 10 Neutron fluence calculated by SMAUG at the same detector locations as in Fig 9.

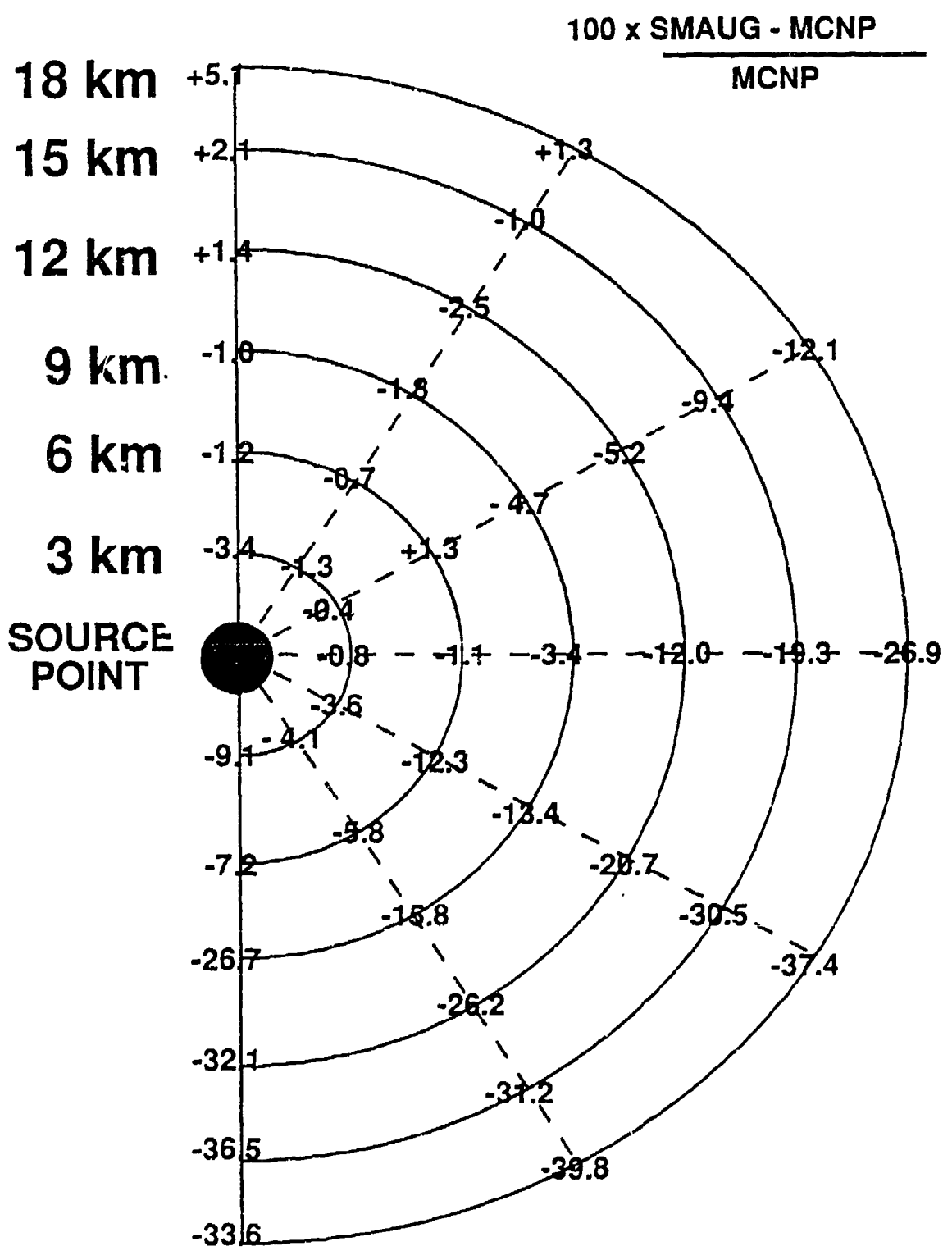

FIGURE 11 Comparison of MCNP and SMAUG calculations of neutron fluence at the same detector locations.

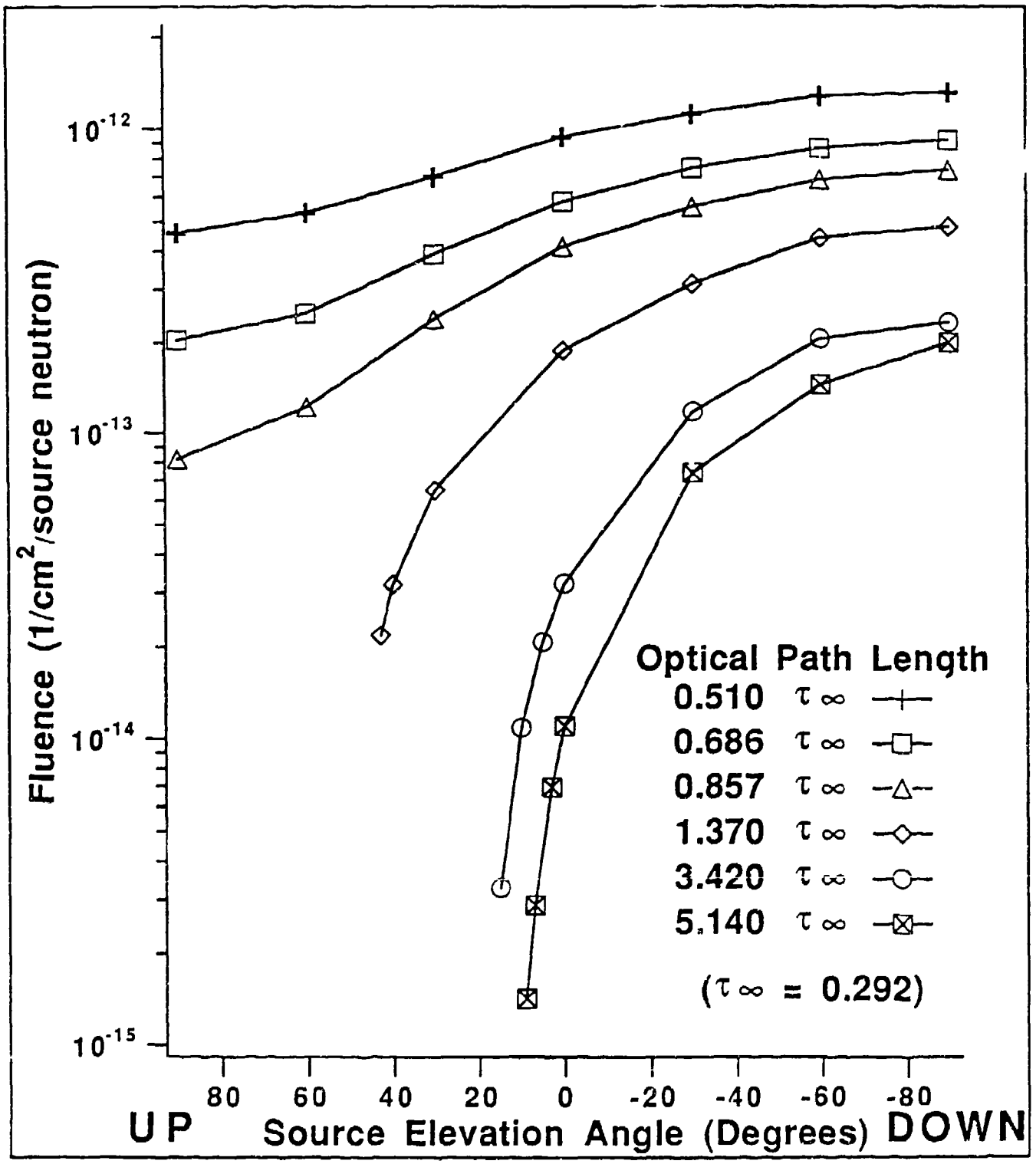

FIGURE 12 Neutron fluence calculated by MCNP using ring detectors on surfaces of constant optical pathlength.

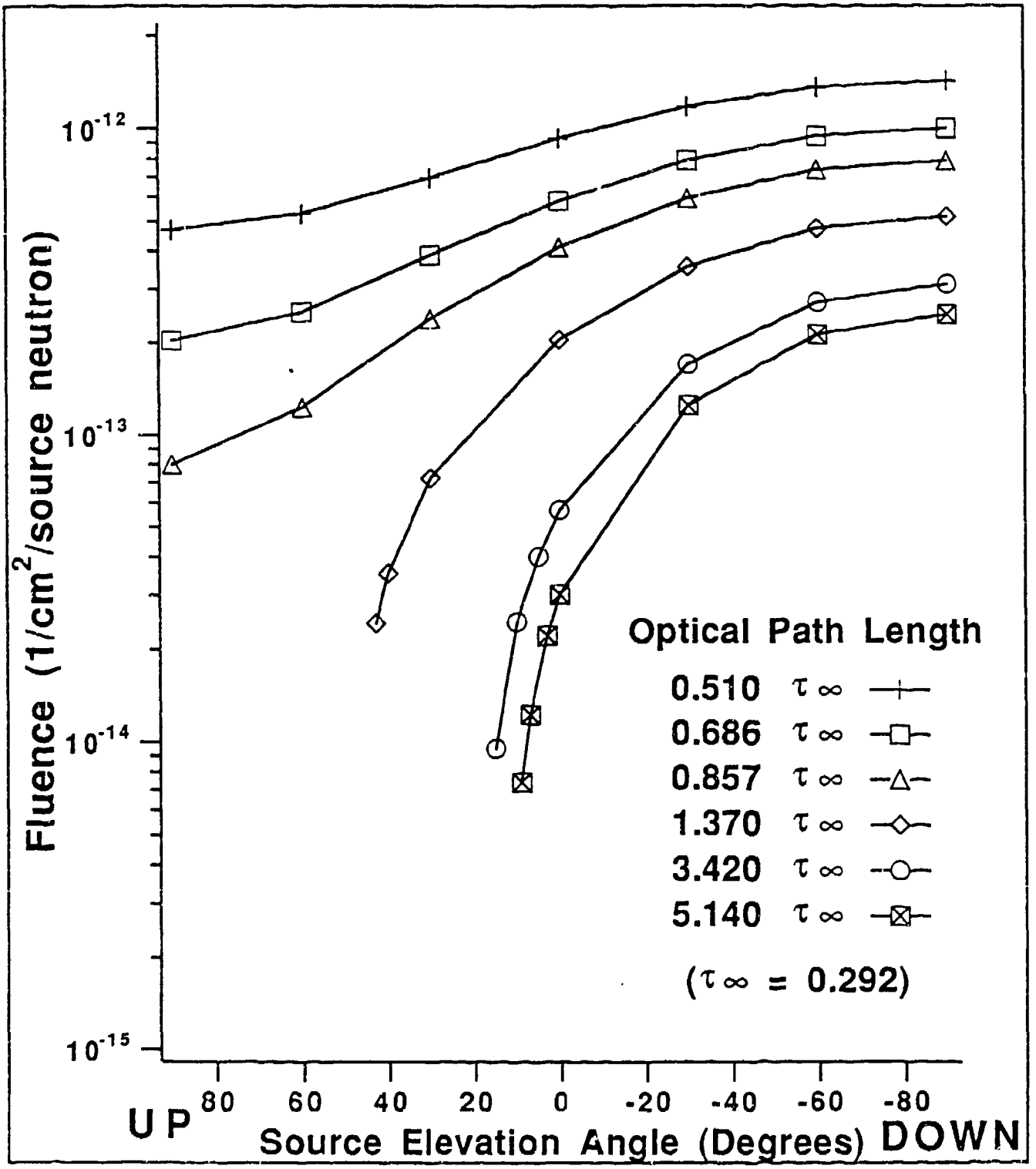

FIGURE 13 Neutron fluence calculated by SMAUG at the same detector locations as in Fig 12.

as a function of source elevation angle are predicted by both SMAUG and MCNP, and the SMAUG results are higher than the MCNP results.

Figure 14 shows a comparison of the MCNP and SMAUG results plotted as a function of range for τ greater than τ_∞, where τ_∞ for a 40 km source altitude equals 0.292 or about 6.5 g/cm^2. Again r^{-2} (spherical divergence) curves are shown on the graphs for comparison. At a τ of $1.37\tau_\infty$, both MCNP and SMAUG display an r^{-2} response. At τ of $3.42\tau_\infty$ and $5.14\tau_\infty$, SMAUG is dead on an r^{-2} response, which should be expected from MIS on surfaces of equal mass integral. At forty kilometers, $5.14\tau_\infty$ equates to about 35 g/cm^2. The MCNP results for these τ fall off faster than r^{-2}, more for positive source elevation angles than negative, which again shows that MIS does not adequately handle the greater escape probability for neutrons travelling up into thinner air.

The errors for the ring detectors on the surfaces of constant optical path length were less than 0.05, with the exception of the results for the two detectors at the farthest ranges which had errors of 0.08 and 0.10. Again these error levels indicate a good confidence level in the MCNP results.

5.1.3 Computational Costs

A critical issue in evaluating the feasibility of using Monte Carlo methods to model radiation transport in the exponential atmosphere is the computational cost of the various runs. An MCNP run of 50,000 source neutrons on the 181 cell geometry without employing any variance reduction techniques or tallies took 60 minutes, or 0.072 seconds per source neutron. An MCNP run of 25,000 source neutrons with geometric splitting and 98 cell average tallies took 400 minutes, 0.96 seconds per source neutron. With geometric splitting a total of 1,273,414 neutrons were tracked. Runs with the ring detectors proved to be much more expensive. A run of 7500 source neutrons with 14 ring detectors took 580 minutes, 4.64 seconds per source neutron. A total of 380,693 total neutrons were tracked. While these run times were long, they were shorter than the mean time between failure of the ELXSI computer at AFIT, which was not true for the low altitude simulations.

Another issue in computational cost is the type of cross section used. MCNP offers the options of continuous cross sections (first order interpolation between points), discrete cross section (zeroth order interpolation between points), and multigroup cross sections. The continuous cross sections should provide the most accurate answers, but will take more

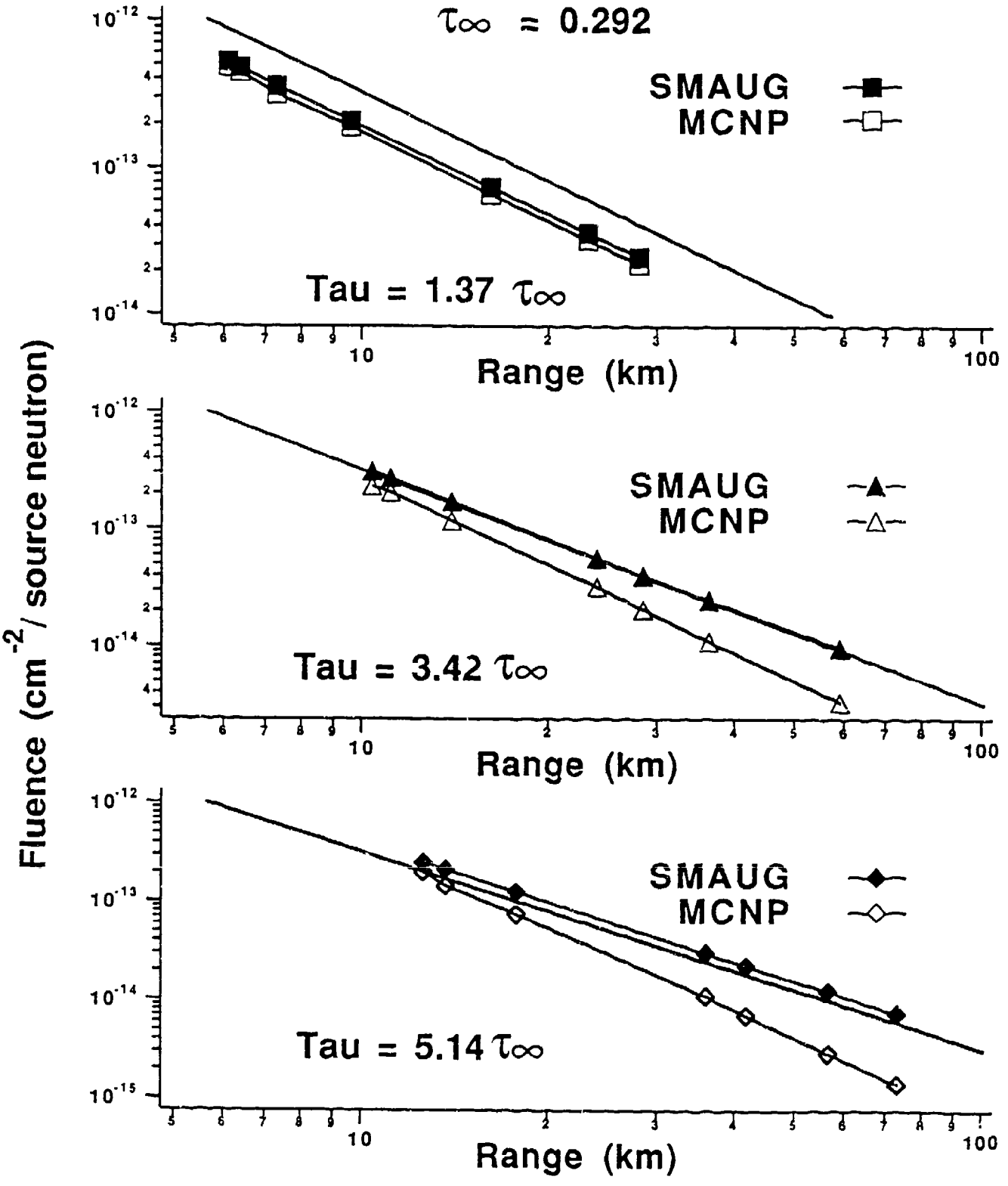

FIGURE 14 Comparison of SMAUG and MCNP calculations for detectors on surfaces of constant optical thickness.

time to run for most elements. The discrete cross sections will run faster in most cases, but not be as accurate. The multigroup cross sections are the smallest so should run the fastest while being less accurate, however the multigroup cross sections have the advantage of being directly transportable to discrete ordinates calculations. All of the MCNP calculations were performed using the discrete cross sections. A test run with one the calculation using the continuous cross sections showed no statistically significant variations between the two calculations, and took the same amount of run time to less than .05%. The time for the calculation was nearly identical because this problem only included nitrogen and oxygen which have no sharp resonances in their cross section; in general use, the continuous cross sections will take more time. We were unable to perform a comparison with the multigroup cross sections because of difficulties getting these cross sections read onto the ELXSI computer.

5.2 Low Altitude Simulation

Several problems arose during the low altitude problem. First, because of the 200 cell limit, the cell sizes were orders of magnitude too large for proper transport of the particles through the medium. Ideally, the cell thickness should be no larger than a mean free path, but this was impossible because of the scale of the problem. Reducing the cell thickness to approximately ten mean free paths (still optically very thick) at the lowest altitudes would mean giving up valuable cells in the higher altitudes. This would have introduced substantial error, since reserving most of the cells to the lower altitudes would have omitted down-scatter from higher altitudes. Reducing the size of the geometry would have made the problem impractical from the standpoint that detector locations would now be severely distance limited. This also would have introduced more error into the problem by increasing the particle leakage from the outer boundaries.

Another major problem encountered during the analysis was the very high importance factors needed to transport the particles from the source region to the outer cell regions, especially at low altitudes where the density is highest. It was determined after many smaller runs that importance factors on the order of 5000 for the lower regions were necessary to transport the neutrons to the farthest cell locations. The result of these high importances was to cause the run times to increase dramatically to the point where no jobs ever finished and final importances could be determined.

Reliability problems with the ELXSI computer were also encountered throughout the entire analysis period. Towards the end of the analysis period after the final geometry configuration was determined, the mean time between failure of the ELXSI computer was less than the run times necessary to complete the geometric splitting/Russian roulette alone, sans tallies and detectors. This was a strong indicator of the impracticality of using Monte Carlo for a problem of this type.

At this time there are no results to report. The most uptodate geometry configuration used is provided on figure 4 and the corresponding input file is listed in Appendix A. It became apparent after much trial and error that analysis of the low altitude problem by Monte Carlo is too impractical. A problem of this type demands a specialized approach and a specialized computer code that can handle the difficulties encountered in this analysis. Some suggestions for future efforts in dealing with this problem in Monte Carlo are:

1. modify an existing Monte Carlo code (e.g. MCNP) to allow variations in material density without specifying vertical cells,

2. with the capability to vary material density without vertical cells, only surfaces in the radial direction are needed to assist in particle transport, and

3. invoke more advanced variance reduction techniques to aid in particle transport and efficiency, some suggestions are path length stretching, iteration on the forward and adjoint solutions, and DXTRAN spheres.

6 Conclusions

With respect to knowledge and insight gained, this project was quite successful. From our efforts in constructing the geometries and cell meshes important to Monte Carlo simulation, and from our iterative variance reduction exercises, we feel that we have generated a significant body of knowledge with regards to applying MCNP to this problem, which someone else can apply and save considerable time and energy in the initial stages of additional research in this problem area.

We have demonstrated, taking into account our approximations of the atmosphere, that SMAUG-II predictions can be accurate within a few percent close to the source point, as well as significantly in error (30-40%) only about 12 kilometers away below the point source due to losses out the top of the atmosphere. Unfortunately, we were unable to look at radiation transport at more considerable distances due to limitations of Monte Carlo simulation, MCNP, and the time available. We were

not able to look at distances farther out than those which relate to the build-up region. The contributions from primary and secondary gammas need to be included in future work in order to present a more comprehensive analysis.

Applying Monte Carlo to this problem demands the trade-off between computational run time and achieving an acceptable resolution to the results. Mapping out the radiation distribution with cell average tallies provides insight into the radiation transport but it is doubtful that comparison with a discrete ordinates solution is possible because the great numbers of cells needed to allow for small cells at long distances is probably computationally impractical. The same difficulty may prevent the use of point or ring detectors at long distances, because most variance reduction methods require cells or surfaces throughout the problem in order to propagate the radiation to field points far from the source with any statistical significance. The transport of radiation in the lower atmosphere is severely limited and should probably not be pursued in future research.

Monte Carlo production codes, including MCNP, have not been constructed to handle this type of problem. A Monte Carlo code designed to this problem would be useful. Limitations such as restrictions on the number of cells allowed and not allowing material density gradients within cells could be eliminated.

References

1. Shulstad, Raymond A. Capt, USAF. "An Evaluation of Mass Integral Scaling as Applied to the Atmospheric Radiation Transport", Doctoral Dissertation, Air Force Institute of Technology, DS/PH/76-3, November 1976.

2. Murphy, Harry M., "A User's Guide to the SMAUG-II Computer Code", Air Force Weapons Laboratory, Kirtland AFB, NM, 4 March 1981.

3. Zerby, C. D., "Radiation Flux Transformation as a Function of Density of an Infinite Medium with Anisotropic Point Sources", Oak Ridge National Laboratory Publication ORNL 2100, Oak Ridge National Laboratory, TN, 1956.

4. RSIC Computer Code Collection CCC-200, "MCNP Version 3B, Monte Carlo Neutron and Photon Transport Code System", March 1989. (Contributed by Los Alamos National Laboratory. See Los Alamos Technical Publication LA-7396-M.)

5. Little, R. C., "Neutron and Photon Multigroup Data Tables for MCNP3B", Los Alamos Memorandum, Los Alamos National Laboratory, 21 April 1987.

6. Booth, Thomas E., "A Sample Problem for Variance Reduction in MCNP", Los Alamos publication LA-10363-MS, Los Alamos National Laboratory, October 1985.

Appendix A: Input Files

This appendix contains input files for MCNP and for SMAUG-II. The following are included:

1. Notes regarding MCNP input file for high altitude case.

2. Listing of high altitude case input file for MCNP. (It cites the notes presented in the previous item.)

3. Input file for SMAUG-II.

Notes From Input File Used In High Altitude Case

N1: The cell numbers correspond to those shown in Fig 4. For the cells up to a height of 100 km, material 1, which is a 79% nitrogen, 21% oxygen mixture is used. The photon importances listed need to be recalculated before acceptable photon tallies can be obtained.

N2: Material 2 is used for these cells, which is a 78% nitrogen 21% oxygen mixture.

N3: Material 3 is used for these cells, which is a 69% nitrogen, 31% oxygen mixture.

N4: Material 4 is used for these cells, which is a 51% nitrogen, 49% oxygen mixture.

N5: CZ describes a cylinder parallel to the z axis with a radius as listed. The units used in MCNP are centimeters, so 10^5 centimeters equals 1 kilometer.

N6: These are the specifications used for a ring detector, tally type 5. The Z after the tally number specifies a ring perpendicular to the z axis at a given radius. The location of the ring is specified by the cylindrical coordinates of the ring, (z,r), and optionally, the radius of the torus. Guidance on the selection of the radius of the ring detector is given in the MCNP manual in the section describing the tally types.

N7: These are the energy bins for MCNP that MCNP will keep track of the fluence. This feature of the detectors can be used to obtain spectral information about the neutrons that reach the ring detectors, even though the ring detector tally only gives the fluence, not energy deposited.

16 MAY 40 KLICK with N/P SPLITS RING detectors TAU_N 3.42 5.14

101	1	-6.770E-5	16 -17 -1	IMP:N=276	IMP:P=95 **$ N1**
102	1	-6.770E-5	16 -17 1 -2	IMP:N=45.4	IMP:P=6.3
103	1	-6.770E-5	16 -17 2 -3	IMP:N=32.0	IMP:P=3.1
104	1	-6.770E-5	16 -17 3 -4	IMP:N=32.1	IMP:P=3.2
105	1	-6.770E-5	16 -17 4 -5	IMP:N=39.8	IMP:P=5
106	1	-6.770E-5	16 -17 5 -6	IMP:N=54.5	IMP:P=4.6
107	1	-6.770E-5	16 -17 6 -7	IMP:N=36.3	IMP:P=6.2
108	1	-6.770E-5	16 -17 7 -8	IMP:N=97.0	IMP:P=10.2
109	1	-6.770E-5	16 -17 8 -9	IMP:N=140	IMP:P=11.9
110	1	-6.770E-5	16 -17 9 -10	IMP:N=165	IMP:P=12.6
111	1	-6.770E-5	16 -17 10 -11	IMP:N=186	IMP:P=11.6
112	1	-6.770E-5	16 -17 11 -12	IMP:N=256	IMP:P=23.7
113	1	-6.770E-5	16 -17 12 -13	IMP:N=396	IMP:P=37.9
114	1	-6.770E-5	16 -17 13 -14	IMP:N=583	IMP:P=24.7
115	1	-6.770E-5	16 -17 14 -15	IMP:N=2309	IMP:P=71.1
201	1	-5.663E-5	17 -18 -1	IMP:N=127.4	IMP:P=40.6
202	1	-5.663E-5	17 -18 1 -2	IMP:N=21.5	IMP:P=4.5
203	1	-5.663E-5	17 -18 2 -3	IMP:N=15.6	IMP:P=2.1
204	1	-5.663E-5	17 -18 3 -4	IMP:N=15.7	IMP:P=2.3
205	1	-5.663E-5	17 -18 4 -5	IMP:N=18.9	IMP:P=2.9
206	1	-5.663E-5	17 -18 5 -6	IMP:N=27.6	IMP:P=2.9
207	1	-5.663E-5	17 -18 6 -7	IMP:N=34.9	IMP:P=3.8
208	1	-5.663E-5	17 -18 7 -8	IMP:N=50	IMP:P=5.9
209	1	-5.663E-5	17 -18 8 -9	IMP:N=71.5	IMP:P=6.9
210	1	-5.663E-5	17 -18 9 -10	IMP:N=78.4	IMP:P=7.4
211	1	-5.663E-5	17 -18 10 -11	IMP:N=90.8	IMP:P=9.2
212	1	-5.663E-5	17 -18 11 -12	IMP:N=140	IMP:P=17.2
213	1	-5.663E-5	17 -18 12 -13	IMP:N=216	IMP:P=21.9
214	1	-5.663E-5	17 -18 13 -14	IMP:N=324	IMP:P=19.6
215	1	-5.663E-5	17 -18 14 -15	IMP:N=1179	IMP:P=71.1
301	1	-4.349E-5	18 -19 -1	IMP:N=53.3	IMP:P=16.2
302	1	-4.349E-5	18 -19 1 -2	IMP:N=10.2	IMP:P=2.8
303	1	-4.349E-5	18 -19 2 -3	IMP:N=7.4	IMP:P=1.5
304	1	-4.349E-5	18 -19 3 -4	IMP:N=7.7	IMP:P=1.5
305	1	-4.349E-5	18 -19 4 -5	IMP:N=9.2	IMP:P=1.8
306	1	-4.349E-5	18 -19 5 -6	IMP:N=13.5	IMP:P=2.2
307	1	-4.349E-5	18 -19 6 -7	IMP:N=17.7	IMP:P=2.8
308	1	-4.349E-5	18 -19 7 -8	IMP:N=25.5	IMP:P=3.2
309	1	-4.349E-5	18 -19 8 -9	IMP:N=35.1	IMP:P=4.1
310	1	-4.349E-5	18 -19 9 -10	IMP:N=37.0	IMP:P=3.9
311	1	-4.349E-5	18 -19 10 -11	IMP:N=46.1	IMP:P=5.3
312	1	-4.349E-5	18 -19 11 -12	IMP:N=78.4	IMP:P=8.8
313	1	-4.349E-5	18 -19 12 -13	IMP:N=125	IMP:P=11.6
314	1	-4.349E-5	18 -19 13 -14	IMP:N=185	IMP:P=11.6
315	1	-4.349E-5	18 -19 14 -15	IMP:N=523	IMP:P=40.6
401	1	-3.043E-5	19 -20 -1	IMP:N=32.8	IMP:P=13.5
402	1	-3.043E-5	19 -20 1 -2	IMP:N=6.7	IMP:P=2.5
403	1	-3.043E-5	19 -20 2 -3	IMP:N=4.8	IMP:P=1.5

```
404  1  -3.043E-5   19 -20  3 -4    IMP:N=5.1    IMP:P=1.4
405  1  -3.043E-5   19 -20  4 -5    IMP:N=6.3    IMP:P=1.5
406  1  -3.043E-5   19 -20  5 -6    IMP:N=8.8    IMP:P=1.7
407  1  -3.043E-5   19 -20  6 -7    IMP:N=12.1   IMP:P=2.4
408  1  -3.043E-5   19 -20  7 -8    IMP:N=17.5   IMP:P=2.5
409  1  -3.043E-5   19 -20  8 -9    IMP:N=23.1   IMP:P=3.1
410  1  -3.043E-5   19 -20  9 -10   IMP:N=24.3   IMP:P=3.1
411  1  -3.043E-5   19 -20  10 -11  IMP:N=31.2   IMP:P=3.9
412  1  -3.043E-5   19 -20  11 -12  IMP:N=51.7   IMP:P=6.7
413  1  -3.043E-5   19 -20  12 -13  IMP:N=78.2   IMP:P=8.5
414  1  -3.043E-5   19 -20  13 -14  IMP:N=125    IMP:P=9.2
415  1  -3.043E-5   19 -20  14 -15  IMP:N=298    IMP:P=27.1
501  1  -2.129E-5   20 -21 -1       IMP:N=24.4   IMP:P=12.1
502  1  -2.129E-5   20 -21  1 -2    IMP:N=4.9    IMP:P=2.2
503  1  -2.129E-5   20 -21  2 -3    IMP:N=3.7    IMP:P=1.5
504  1  -2.129E-5   20 -21  3 -4    IMP:N=4.1    IMP:P=1.5
505  1  -2.129E-5   20 -21  4 -5    IMP:N=5.3    IMP:P=1.4
506  1  -2.129E-5   20 -21  5 -6    IMP:N=7.1    IMP:P=1.7
507  1  -2.129E-5   20 -21  6 -7    IMP:N=10     IMP:P=2.0
508  1  -2.129E-5   20 -21  7 -8    IMP:N=13.7   IMP:P=2.4
509  1  -2.129E-5   20 -21  8 -9    IMP:N=18     IMP:P=2.6
510  1  -2.129E-5   20 -21  9 -10   IMP:N=19.5   IMP:P=2.8
511  1  -2.129E-5   20 -21 10 -11   IMP:N=25.1   IMP:P=3.1
512  1  -2.129E-5   20 -21 11 -12   IMP:N=41.1   IMP:P=5.7
513  1  -2.129E-5   20 -21 12 -13   IMP:N=59.7   IMP:P=7.9
514  1  -2.129E-5   20 -21 13 -14   IMP:N=105    IMP:P=9
515  1  -2.129E-5   20 -21 14 -15   IMP:N=233    IMP:P=17.8
601  1  -1.266E-5   21 -22 -1       IMP:N=9.5    IMP:P=8.5
602  1  -1.266E-5   21 -22  1 -2    IMP:N=2.5    IMP:P=1.8
603  1  -1.266E-5   21 -22  2 -3    IMP:N=2.2    IMP:P=1.2
604  1  -1.266E-5   21 -22  3 -4    IMP:N=2.6    IMP:P=1.1
605  1  -1.266E-5   21 -22  4 -5    IMP:N=3.4    IMP:P=1.1
606  1  -1.266E-5   21 -22  5 -6    IMP:N=4.6    IMP:P=1.3
607  1  -1.266E-5   21 -22  6 -7    IMP:N=6.3    IMP:P=1.5
608  1  -1.266E-5   21 -22  7 -8    IMP:N=8.6    IMP:P=1.8
609  1  -1.266E-5   21 -22  8 -9    IMP:N=11.3   IMP:P=1.9
610  1  -1.266E-5   21 -22  9 -10   IMP:N=13.0   IMP:P=2.3
611  1  -1.266E-5   21 -22 10 -11   IMP:N=17.9   IMP:P=2.5
612  1  -1.266E-5   21 -22 11 -12   IMP:N=27.9   IMP:P=3.9
613  1  -1.266E-5   21 -22 12 -13   IMP:N=42.7   IMP:P=5.6
614  1  -1.266E-5   21 -22 13 -14   IMP:N=68.7   IMP:P=7.0
615  1  -1.266E-5   21 -22 14 -15   IMP:N=137    IMP:P=10.3
701  1  -6.187E-6   22 -23 -1       IMP:N=1.8    IMP:P=8.0
702  1  -6.187E-6   22 -23  1 -2    IMP:N=1.5    IMP:P=1.9
703  1  -6.187E-6   22 -23  2 -3    IMP:N=1.9    IMP:P=1.42
704  1  -6.187E-6   22 -23  3 -4    IMP:N=2.5    IMP:P=1.3
705  1  -6.187E-6   22 -23  4 -5    IMP:N=3.3    IMP:P=1.4
706  1  -6.187E-6   22 -23  5 -6    IMP:N=4.5    IMP:P=1.4
707  1  -6.187E-6   22 -23  6 -7    IMP:N=6      IMP:P=1.6
```

```
708   1  -6.187E-6   22 -23  7 -8    IMP:N=7.9    IMP:P=1.8
709   1  -6.187E-6   22 -23  8 -9    IMP:N=10.4   IMP:P=2.1
710   1  -6.187E-6   22 -23  9 -10   IMP:N=11.8   IMP:P=2.5
711   1  -6.187E-6   22 -23 10 -11   IMP:N=16.3   IMP:P=2.5
712   1  -6.187E-6   22 -23 11 -12   IMP:N=25.5   IMP:P=3.4
713   1  -6.187E-6   22 -23 12 -13   IMP:N=40.5   IMP:P=5
714   1  -6.187E-6   22 -23 13 -14   IMP:N=62.1   IMP:P=6.3
715   1  -6.187E-6   22 -23 14 -15   IMP:N=107    IMP:P=8.5
801   1  -3.034E-6   23 -24 -1       IMP:N=1      IMP:P=8.2
802   1  -3.034E-6   23 -24  1 -2    IMP:N=1.5    IMP:P=2.2
803   1  -3.034E-6   23 -24  2 -3    IMP:N=2.0    IMP:P=1.7
804   1  -3.034E-6   23 -24  3 -4    IMP:N=2.6    IMP:P=1.6
805   1  -3.034E-6   23 -24  4 -5    IMP:N=3.5    IMP:P=1.7
806   1  -3.034E-6   23 -24  5 -6    IMP:N=4.5    IMP:P=1.7
807   1  -3.034E-6   23 -24  6 -7    IMP:N=5.7    IMP:P=1.9
808   1  -3.034E-6   23 -24  7 -8    IMP:N=7.4    IMP:P=2.2
809   1  -3.034E-6   23 -24  8 -9    IMP:N=9.4    IMP:P=2.5
810   1  -3.034E-6   23 -24  9 -10   IMP:N=10.8   IMP:P=2.4
811   1  -3.034E-6   23 -24 10 -11   IMP:N=14.4   IMP:P=2.5
812   1  -3.034E-6   23 -24 11 -12   IMP:N=22.6   IMP:P=3.6
813   1  -3.034E-6   23 -24 12 -13   IMP:N=33.1   IMP:P=5
814   1  -3.034E-6   23 -24 13 -14   IMP:N=48.4   IMP:P=6.5
815   1  -3.034E-6   23 -24 14 -15   IMP:N=80.9   IMP:P=8.6
901   1  -1.485E-6   24 -25 -1       IMP:N=13.5   IMP:P=19
902   1  -1.485E-6   24 -25  1 -2    IMP:N=3.3    IMP:P=3.8
903   1  -1.485E-6   24 -25  2 -3    IMP:N=2.9    IMP:P=2.6
904   1  -1.485E-6   24 -25  3 -4    IMP:N=3.3    IMP:P=2.1
905   1  -1.485E-6   24 -25  4 -5    IMP:N=4      IMP:P=2.1
906   1  -1.485E-6   24 -25  5 -6    IMP:N=5      IMP:P=1.8
907   1  -1.485E-6   24 -25  6 -7    IMP:N=6.2    IMP:P=2.0
908   1  -1.485E-6   24 -25  7 -8    IMP:N=7.7    IMP:P=2.1
909   1  -1.485E-6   24 -25  8 -9    IMP:N=9.6    IMP:P=2.6
910   1  -1.485E-6   24 -25  9 -10   IMP:N=10.8   IMP:P=2.5
911   1  -1.485E-6   24 -25 10 -11   IMP:N=13.4   IMP:P=2.6
912   1  -1.485E-6   24 -25 11 -12   IMP:N=19.8   IMP:P=3.6
913   1  -1.485E-6   24 -25 12 -13   IMP:N=28.9   IMP:P=4.4
914   1  -1.485E-6   24 -25 13 -14   IMP:N=43.7   IMP:P=6
915   1  -1.485E-6   24 -25 14 -15   IMP:N=70.6   IMP:P=8.6
1001  1  -5.415E-7   25 -26 -1       IMP:N=34.6   IMP:P=31.6
1002  1  -5.415E-7   25 -26  1 -2    IMP:N=6.2    IMP:P=5.6
1003  1  -5.415E-7   25 -26  2 -3    IMP:N=3.8    IMP:P=2.8
1004  1  -5.415E-7   25 -26  3 -4    IMP:N=3.3    IMP:P=2
1005  1  -5.415E-7   25 -26  4 -5    IMP:N=3.4    IMP:P=2
1006  1  -5.415E-7   25 -26  5 -6    IMP:N=3.7    IMP:P=1.8
1007  1  -5.415E-7   25 -26  6 -7    IMP:N=4.2    IMP:P=1.8
1008  1  -5.415E-7   25 -26  7 -8    IMP:N=4.8    IMP:P=1.8
1009  1  -5.415E-7   25 -26  8 -9    IMP:N=5.6    IMP:P=1.8
1010  1  -5.415E-7   25 -26  9 -10   IMP:N=6.2    IMP:P=1.7
1011  1  -5.415E-7   25 -26  10 -11  IMP:N=7.5    IMP:P=1.8
```

```
1012  1  -5.415E-7   25 -26  11 -12 IMP:N=10.3   IMP:P=2.2
1013  1  -5.415E-7   25 -26  12 -13 IMP:N=14.2   IMP:P=2.7
1014  1  -5.415E-7   25 -26  13 -14 IMP:N=19.9   IMP:P=13.6
1015  1  -5.415E-7   25 -26  14 -15 IMP:N=27.8   IMP:P=14.6
1101  1  -8.038E-8   26 -27  -1      IMP:N=86.4   IMP:P=81.3
1102  1  -8.038E-8   26 -27   1  -3  IMP:N=6.9    IMP:P=4.6
1103  1  -8.038E-8   26 -27   3  -5  IMP:N=3.6    IMP:P=1.9
1104  1  -8.038E-8   26 -27   5  -7  IMP:N=3.1    IMP:P=1.4
1105  1  -8.038E-8   26 -27   7  -9  IMP:N=3.2    IMP:P=1.3
1106  1  -8.038E-8   26 -27   9 -11  IMP:N=3.3    IMP:P=1.1
1107  1  -8.038E-8   26 -27  11 -13  IMP:N=4.6    IMP:P=1.2
1108  1  -8.038E-8   26 -27  13 -15  IMP:N=7.3    IMP:P=1.7
1201  1  -4.619E-9   27 -28  -1      IMP:N=299    IMP:P=114
1202  1  -4.619E-9   27 -28   1  -3  IMP:N=19.2   IMP:P=11.2
1203  1  -4.619E-9   27 -28   3  -5  IMP:N=8.3    IMP:P=4.7
1204  1  -4.619E-9   27 -28   5  -7  IMP:N=5.9    IMP:P=2.8
1205  1  -4.619E-9   27 -28   7  -9  IMP:N=5      IMP:P=2.0
1206  1  -4.619E-9   27 -28   9 -11  IMP:N=3.9    IMP:P=1.4
1207  1  -4.619E-9   27 -28  11 -13  IMP:N=4.3    IMP:P=1.4
1208  1  -4.619E-9   27 -28  13 -15  IMP:N=5.7    IMP:P=1.6
1301  2  -8.013E-12  28 -29  -1      IMP:N=508    IMP:P=190   $ N2
1302  2  -8.013E-12  28 -29   1  -5  IMP:N=12.8   IMP:P=7.0
1303  2  -8.013E-12  28 -29   5  -9  IMP:N=5.2    IMP:P=2.3
1304  2  -8.013E-12  28 -29   9 -12  IMP:N=3.3    IMP:P=1.2
1305  2  -8.013E-12  28 -29  12 -15  IMP:N=3.1    IMP:P=1
1401  3  -6.439E-14  29 -30  -1      IMP:N=1847   IMP:P=569
1402  3  -6.439E-14  29 -30   1  -5  IMP:N=37.6   IMP:P=19.6
1403  3  -6.439E-14  29 -30   5  -9  IMP:N=13.6   IMP:P=15.6
1404  3  -6.439E-14  29 -30   9 -12  IMP:N=6.6    IMP:P=2.7   $ N3
1405  3  -6.439E-14  29 -30  12 -15  IMP:N=4.9    IMP:P=1.7
1501  4  -3.187E-15  30 -31  -1      IMP:N=2770   IMP:P=569   $ N4
1502  4  -3.187E-15  30 -31   1  -5  IMP:N=72.7   IMP:P=43.2
1503  4  -3.187E-15  30 -31   5  -9  IMP:N=25.5   IMP:P=9.5
1504  4  -3.187E-15  30 -31   9 -12  IMP:N=10.7   IMP:P=4.2
1505  4  -3.187E-15  30 -31  12 -15  IMP:N=6.8    IMP:P=2.6
999   0              31:-16:15       IMP:N=0      IMP:P=0  $ OUTSIDE WORLD

C    15 CONCENTRIC CYLINDERS   16 PLANES PERPENDICULAR TO Z AXIS
1    CZ  2.5E+5          $ N5
2    CZ  7.5E+5
3    CZ  12.5E+5
4    CZ  17.5E+5
5    CZ  22.5E+5
6    CZ  27.5E+5
7    CZ  32.5E+5
8    CZ  37.5E+5
9    CZ  42.5E+5
10   CZ  50.0E+5
11   CZ  60.0E+5
```

```
12   CZ 70.0E+5
13   CZ 80.0E+5
14   CZ 90.0E+5
15   CZ 100.0E+5
16   PZ 20.0E+5
17   PZ 21.25E+5
18   PZ 22.5E+5
19   PZ 25.0E+5
20   PZ 27.5E+5
21   PZ 30.0E+5
22   PZ 35.0E+5
23   PZ 40.0E+5
24   PZ 45.0E+5
25   PZ 50.0E+5
26   PZ 60.0E+5
27   PZ 80.0E+5
28   PZ 100.0E+5
29   PZ 150.0E+5
30   PZ 200.0E+5
31   PZ 300.0E+5

MODE N P
C       ISOTROPIC FISSION SOURCE AT (0,0,50 klicks)
SDEF  ERG=D1 POS=0 0 40.05E+5 CEL=801
SC1     FISSION SPECTRUM (GENERIC)
SI1  H 4.14E-7 1.1254E-6 3.059E-6 1.0677E-5 2.9023E-5 1.013E-4 5.8295E-4
     1.2341E-3 3.3546E-3 1.0333E-2 2.1875E-2 2.4788E-2 5.2475E-2
     0.1111 0.1576 0.5502 1.108 1.827 2.307 2.385
     3.012 4.066 4.724 4.966 6.376 7.408 8.187
     9.048 10.00 11.05 12.21 12.82 13.84 14.19
SP1  D 0 0 0 0 0 2.0226E-3 2.3974E-2
     4.2300E-2 7.9823E-2 1.1337E-1 8.4647E-2 1.4145E-2 8.1805E-2
     7.0979E-2 3.3869E-2 9.8584E-2 8.4961E-2 6.2051E-2 2.5916E-2 3.6882E-3
     2.2402E-2 2.6063E-2 1.2918E-2 4.0545E-3 1.8073E-2 8.6953E-3 5.8951E-3
     6.1457E-3 7.8970E-3 9.4915E-3 1.6382E-2 1.7368E-2 3.3667E-2 9.3298E-3
C       MATERIAL SPECIFICATION
M1    7014.04D  -0.79    $ DISCRETE NITROGEN XSEC
      8016.30D  -0.21    $ DISCRETE OXYGEN XSEC
M2    7014.04D  -0.78    $ DISCRETE NITROGEN XSEC
      8016.30D  -0.22    $ DISCRETE OXYGEN XSEC
M3    7014.04D  -0.69    $ DISCRETE NITROGEN XSEC
      8016.30D  -0.31    $ DISCRETE OXYGEN XSEC
M4    7014.04D  -0.51    $ DISCRETE NITROGEN XSEC
       8016.30D  -0.49    $ DISCRETE OXYGEN XSEC
C    18000.01D -0.01    $ omitted don't have Ar Xsec with gammas!!!
PHYS:N,P  14.2    $ CROSS SECTIONS ABOVE 14.2 MEV WILL BE EXPUNGED.
C
C       TALLY CARDS
C       NEUTRON (1/cm2) from ring detectors
```

```
C     AT tau_norm's of 3.42  5.14
F5Z:N    55.34E5   57.05E5   0.1E5          $ N6
F15Z:N   46.38E5   35.92E5   0.1E5
F25Z:N   42.53E5   28.40E5   0.1E5
F35Z:N   40.05E5   24.00E5   0.1E5
F45Z:N   33.06E5   12.11E5   0.1E5
F55Z:N   30.40E5    5.57E5   0.1E5
F65Z:N   29.63E5    0.1E5    0.1E5
F75Z:N   51.48E5   72.14E5   0.1E5
F85Z:N   46.95E5   56.18E5   0.1E5
F95Z:N   42.24E5   41.88E5   0.1E5
F105Z:N  40.05E5   36.00E5   0.1E5
F115Z:N  31.14E5   15.43E5   0.1E5
F125Z:N  28.18E5    6.85E5   0.1E5
F135Z:N  27.34E5    0.1E5    0.1E5
C
F2:N    31   $ LEAKAGE OUT OF THE TOP SURFACE
C
C     OUTPUT ENERGY BIN STRUCTURE (MeV)
E5    2.50E-8  2 10  14.2     $ N7
E15   2.50E-8  2 10  14.2
E25   2.50E-8  2 10  14.2
E35   2.50E-8  2 10  14.2
E45   2.50E-8  2 10  14.2
E55   2.50E-8  2 10  14.2
E65   2.50E-8  2 10  14.2
E75   2.50E-8  2 10  14.2
E85   2.50E-8  2 10  14.2
E95   2.50E-8  2 10  14.2
E105  2.50E-8  2 10  14.2
E115  2.50E-8  2 10  14.2
E125  2.50E-8  2 10  14.2
E135  2.50E-8  2 10  14.2
C
E2:N   2.50E-8  2 10  14.2
C
NPS  10000  $ RUN 10000 HISTORIES.
PRINT     $ PRINT ALL POSSIBLE OUTPUT FOR EASIER DEBUGGING.
```

```
 PAGE   1       S M A U G - I I
1  (title=Example of SMAUG-II Input                                    )
2  (read neutron                                                       )
       File specification is: TNS.NEU
(0.0       1.1315-4 9.8489-3 9.3298-3 3.3667-2 1.7368-2 1.6382-2 9.4915-3)
(7.8970-3 6.1457-3 5.8951-3 8.6953-3 1.8073-2 4.0545-3 1.2918-2 2.6063-2)
(2.2402-2 3.6882-3 2.5916-2 6.2051-2 8.4961-2 9.8584-2 3.3869-2 7.0979-2)
(8.1805-2 1.4145-2 8.4647-2 1.1337-1 7.9823-2 4.2300-2 2.3974-2 2.0226-3)
(0.0       0.0       0.0       0.0       0.0     RSIC-36 (page 71) TNS. Neut.)
3  (norm n=1                                                           )
4  (read gamma                                                         )
       File specification is: EXP.GAM
(1.6496-5 1.3403-4 3.0209-4 9.0754-4 2.7264-3 8.1905-3 2.4605-2 2.7044-2)
(4.6875-2 8.1246-2 1.4082-1 1.3014-1 1.4655-1 1.0935-1 1.2896-1 4.7940-2)
(3.0055-2 2.5815-2 1.5833-2 1.0701-2 1.0820-2 1.1*EXP(-1.1*En). 10Nov81.)
5  (norm g=1                                                           )
6  (yield=1                                                            )
7  (hob=40050                                                          )
8  (alt=40050                                                          )
9  (ran=36000                                                          )
10  (go                                                                )
```

Explanation of Control Statements:

title=	Title of the problem
read neutron	Read neutron source spectrum
norm n=	Normalize the neutron yield
read gamma	Read gamma source spectrum
norm g=	Normalize the gamma yield
yield=	Detonation yields
hob=	Height of bursts
alt=	Reciever Altitudes
ran=	Ground ranges
go	Do the calculations specified

Appendix B: Data Tables

This appendix contains the MCNP results for the high altitude test case which are summarized in the figures in the body of the report. Tabulated data includes the following:

1. Ring detector results for locations on surfaces of constant optical depth from the source point. For comparison, SMAUG-II data is also provided.

2. Ring detector results for locations on surfaces of constant range from the source point. For comparison, SMAUG-II data is also provided.

3. Cell average results for cells in various layers (of constant altitude), including layers above and layers below the source point altitude.

TAU = 0.51 TAU INFINITY

ELEVATION ANGLE (Degrees)	r (km)	z (km)	SLANT RANGE (km)	MCNP FLUENCE (1/cm2)	MCNP ERROR (Fraction)	SMAUG FLUENCE (1/cm2)
90	0.1	45.10	5.05	4.549E-13	0.0196	4.675E-13
60	2.38	44.17	4.75	5.273E-13	0.0137	5.270E-13
30	3.61	42.13	3.61	6.877E-13	0.0091	6.873E-13
0	3.60	40.05	3.60	9.250E-13	0.0092	9.208E-13
-30	2.77	38.45	3.20	1.100E-12	0.0117	1.167E-13
-60	1.49	37.47	2.98	1.265E-12	0.0126	1.347E-12
-90	0.1	37.14	2.91	1.295E-12	0.0146	1.412E-12

TAU = 0.686 TAU INFINITY

ELEVATION ANGLE (Degrees)	r (km)	z (km)	SLANT RANGE (km)	MCNP FLUENCE (1/cm2)	MCNP ERROR (Fraction)	SMAUG FLUENCE (1/cm2)
90	0.1	48.15	8.10	2.021E-13	0.0121	2.027E-13
60	3.64	46.36	7.28	2.475E-13	0.0091	2.504E-13
30	5.09	42.99	5.88	3.861E-13	0.0099	3.841E-13
0	4.80	40.05	4.80	5.704E-13	0.0091	5.765E-13
-30	3.57	37.99	4.12	7.311E-13	0.0160	7.827E-13
-60	1.88	36.79	3.76	8.505E-13	0.0158	9.406E-13
-90	0.1	36.39	3.66	9.063E-13	0.0199	9.957E-13

TAU = 0.857 TAU INFINITY

ELEVATION ANGLE (Degrees)	r (km)	z (km)	SLANT RANGE (km)	MCNP FLUENCE (1/cm2)	MCNP ERROR (Fraction)	SMAUG FLUENCE (1/cm2)
90	0.1	53.67	13.62	8.148E-14	0.0099	7.970E-14
60	5.48	49.54	10.96	1.208E-13	0.0093	1.224E-13
30	6.78	43.97	7.83	2.367E-13	0.0145	2.386E-13
0	6.00	40.05	6.00	4.079E-13	0.0127	4.070E-13
-30	4.32	37.55	5.00	5.487E-13	0.0162	5.895E-13
-60	2.24	36.16	4.49	6.725E-13	0.0164	7.309E-13
-90	0.1	35.71	4.34	7.250E-13	0.0311	7.830E-13

TAU = 1.37 TAU INFINITY

ELEVATION ANGLE (Degrees)	r (km)	z (km)	SLANT RANGE (km)	MCNP FLUENCE (1/cm2)	MCNP ERROR (Fraction)	SMAUG FLUENCE (1/cm2)
43	20.55	59.17	28.07	2.172E-14	0.0091	2.430E-14
40	17.79	54.93	23.20	3.175E-14	0.0091	3.534E-14
30	14.0	48.10	16.15	6.453E-14	0.0102	7.200E-14
0	9.6	40.05	9.6	1.867E-13	0.0126	2.034E-13
-30	6.33	36.34	7.3	3.084E-13	0.0175	3.518E-13
-60	3.16	34.52	6.37	4.355E-13	0.0272	4.701E-13
-90	0.1	33.95	6.10	4.739E-13	0.0545	5.144E-13

TAU = 3.42 TAU INFINITY

ELEVATION ANGLE (Degrees)	r (km)	z (km)	SLANT RANGE (km)	MCNP FLUENCE (1/cm2)	MCNP ERROR (Fraction)	SMAUG FLUENCE (1/cm2)
15	57.05	55.34	59.1	3.253E-15	0.0123	9.446E-15
10	35.92	46.38	36.5	1.075E-14	0.0131	2.445E-14
5	28.40	42.53	28.5	2.056E-14	0.0153	3.997E-14
0	24.0	40.05	24.0	3.206E-14	0.0173	5.644E-14
-30	12.11	33.06	14.0	1.164E-13	0.0271	1.690E-13
-60	5.57	30.4	11.14	2.036E-13	0.0325	2.692E-13
-90	0.1	29.63	10.4	2.308E-13	0.0557	3.090E-13

TAU = 5.14 TAU INFINITY

ELEVATION ANGLE (Degrees)	r (km)	z (km)	SLANT RANGE (km)	MCNP FLUENCE (1/cm2)	MCNP ERROR (Fraction)	SMAUG FLUENCE (1/cm2)
9	72.14	51.48	73.0	1.402E-15	0.0137	7.332E-15
7	56.18	46.98	56.6	2.855E-15	0.0155	1.217E-14
3	41.88	42.24	41.9	6.891E-15	0.0213	2.214E-14
0	36.0	40.05	36.0	1.092E-14	0.0192	3.006E-14
-30	15.43	31.14	17.8	7.364E-14	0.0288	1.244E-13
-60	6.85	28.18	13.7	1.434E-13	0.0342	2.117E-13
-90	0.1	27.34	12.6	1.984E-13	0.0889	2.467E-13

SLANT RANGE = 12.0 km

ELEVATION ANGLE (Degrees)	r (km)	z (km)	SLANT RANGE (km)	MCNP FLUENCE (1/cm2)	MCNP ERROR (Fraction)	SMAUG FLUENCE (1/cm2)
90	0.1	52.05	12.0	1.018E-13	0.0120	1.003E-13
60	6.0	50.44	12.0	1.016E-13	0.1000	1.042E-13
30	10.39	46.05	12.0	1.119E-13	0.0118	1.181E-13
0	12.0	40.05	12.0	1.307E-13	0.0169	1.486E-13
-30	10.39	34.05	12.0	1.583E-13	0.0293	1.998E-13
-60	6.0	29.66	12.0	1.841E-13	0.0351	2.495E-13
-90	0.1	28.05	12.0	1.807E-13	0.0825	2.661E-13

SLANT RANGE = 15.0 km

ELEVATION ANGLE (Degrees)	r (km)	z (km)	SLANT RANGE (km)	MCNP FLUENCE (1/cm2)	MCNP ERROR (Fraction)	SMAUG FLUENCE (1/cm2)
90	0.1	55.05	15.0	6.821E-14	0.0099	6.678E-14
60	7.5	53.04	15.0	6.916E-14	0.0101	6.988E-14
30	13.0	47.55	15.0	7.381E-14	0.0131	8.143E-14
0	15.0	40.05	15.0	8.806E-14	0.0178	1.091E-14
-30	13.0	32.55	15.0	1.084E-13	0.0306	1.558E-13
-60	7.5	27.06	15.0	1.255E-13	0.0578	1.824E-13
-90	0.1	25.05	15.0	1.137E-13	0.1050	1.791E-13

SLANT RANGE = 18.0 km

ELEVATION ANGLE (Degrees)	r (km)	z (km)	SLANT RANGE (km)	MCNP FLUENCE (1/cm2)	MCNP ERROR (Fraction)	SMAUG FLUENCE (1/cm2)
90	0.1	58.05	18.0	5.004E-14	0.0106	4.762E-14
60	9.0	55.64	18.0	5.080E-14	0.0108	5.015E-14
30	15.59	49.05	18.0	5.261E-14	0.0120	5.987E-14
0	18.0	40.05	18.0	6.202E-14	0.0179	8.842E-14
-30	15.59	31.05	18.0	7.668E-14	0.0315	1.225E-13
-60	9.0	24.46	18.0	6.744E-14	0.0491	1.120E-13
-90	0.1	22.05	18.0	5.881E-14	0.1201	8.854E-14

SLANT RANGE = 3.0 km

ELEVATION ANGLE (Degrees)	r (km)	z (km)	SLANT RANGE (km)	MCNP FLUENCE (1/cm2)	MCNP ERROR (Fraction)	SMAUG FLUENCE (1/cm2)
90	0.1	43.05	3.0	1.145E-12	0.0138	1.185E-12
60	1.50	42.65	3.0	1.176E-12	0.0110	1.193E-12
30	2.60	41.55	3.0	1.211E-12	0.0094	1.216E-12
0	3.00	40.05	3.0	1.262E-12	0.0104	1.252E-12
-30	2.60	38.55	3.0	1.249E-12	0.0145	1.296E-12
-60	1.50	37.45	3.0	1.278E-12	0.0165	1.332E-12
-90	0.1	37.05	3.0	1.225E-12	0.0195	1.374E-12

SLANT RANGE = 6.0 km

ELEVATION ANGLE (Degrees)	r (km)	z (km)	SLANT RANGE (km)	MCNP FLUENCE (1/cm2)	MCNP ERROR (Fraction)	SMAUG FLUENCE (1/cm2)
90	0.1	46.05	6.0	3.406E-13	0.0126	3.448E-13
60	3.0	45.24	6.0	3.485E-13	0.0128	3.511E-13
30	5.20	43.05	6.0	3.761E-13	0.0138	3.712E-13
0	6.0	40.05	6.0	4.025E-13	0.0132	4.069E-13
-30	5.20	37.05	6.0	4.045E-13	0.0157	4.560E-13
-60	3.0	34.85	6.0	4.747E-13	0.0265	5.037E-13
-90	0.1	31.05	6.0	4.862E-13	0.0411	5.241E-13

SLANT RANGE = 9.0 km

ELEVATION ANGLE (Degrees)	r (km)	z (km)	SLANT RANGE (km)	MCNP FLUENCE (1/cm2)	MCNP ERROR (Fraction)	SMAUG FLUENCE (1/cm2)
90	0.1	49.05	9.0	1.665E-13	0.0119	1.681E-13
60	4.5	47.84	9.0	1.698E-13	0.0100	1.730E-13
30	7.79	44.55	9.0	1.808E-13	0.0115	1.898E-13
0	9.0	40.05	9.0	2.155E-13	0.0157	2.230E-13
-30	7.79	35.55	9.0	2.380E-13	0.0212	2.748E-13
-60	4.5	32.25	9.0	2.772E-13	0.0351	3.293E-13
-90	0.1	31.05	9.0	2.587E-13	0.0431	3.527E-13

HEIGHT = 55.0 km

CELL NUMBER	GROUND RANGE (km)	SLANT RANGE (km)	ENERGY DEPOSITED (MeV/g)	MCNP ERROR (Fraction)
1001	1.25	15.00	1.362E-15	0.1042
1002	5.0	15.76	8.312E-16	0.0469
1003	10.0	17.98	6.517E-16	0.0350
1004	15.0	21.18	4.801E-16	0.0309
1005	20.0	24.97	3.322E-16	0.0303
1006	25.0	29.13	2.405E-16	0.0309
1007	30.0	33.52	1.892E-16	0.0330
1008	35.0	38.06	1.397E-16	0.0346
1009	40.0	42.70	1.107E-16	0.0362
1010	46.25	48.60	8.618E-17	0.0373
1011	55.0	57.00	5.762E-17	0.0390
1012	65.0	66.70	3.884E-17	0.0423
1013	75.0	76.47	2.667E-17	0.0442
1014	85.0	86.30	1.881E-17	0.0469

HEIGHT = 47.5 km

CELL NUMBER	GROUND RANGE (km)	SLANT RANGE (km)	ENERGY DEPOSITED (MeV/g)	MCNP ERROR (Fraction)
901	1.25	7.55	3.758E-15	0.0635
902	5.0	8.97	2.423E-15	0.0309
903	10.0	12.47	1.317E-15	0.0297
904	15.0	16.74	7.298E-16	0.0322
905	20.0	21.34	4.600E-16	0.0345
906	25.0	26.08	3.130E-16	0.0365
907	30.0	30.91	2.175E-16	0.0391
908	35.0	35.78	1.609E-16	0.0414
909	40.0	40.69	1.171E-16	0.0440
910	46.25	46.84	8.024E-17	0.0469
911	55.0	55.50	5.980E-17	0.0480
912	65.0	65.42	3.139E-17	0.0495
913	75.0	75.37	1.995E-17	0.0533
914	85.0	85.32	1.317E-17	0.0556

HEIGHT = 42.5 km

CELL NUMBER	GROUND RANGE (km)	SLANT RANGE (km)	ENERGY DEPOSITED (MeV/g)	MCNP ERROR (Fraction)
801	1.25	2.753	4.314E-14	0.0166
802	5.0	5.57	6.588E-15	0.0190
803	10.0	10.29	2.035E-15	0.0240
804	15.0	15.20	9.366E-16	0.0284
805	20.0	20.15	5.420E-16	0.0310
806	25.0	25.11	3.445E-16	0.0339
807	30.0	30.10	2.281E-16	0.0360
808	35.0	35.08	1.593E-16	0.0387
809	40.0	40.07	1.127E-16	0.0414
810	46.25	46.31	7.785E-17	0.0441
811	55.0	55.05	4.836E-17	0.0479
812	65.0	65.04	3.022E-17	0.0529
813	75.0	75.04	1.929E-17	0.0580
814	85.0	85.03	1.224E-17	0.0629

HEIGHT = 37.5 km

CELL NUMBER	GROUND RANGE (km)	SLANT RANGE (km)	ENERGY DEPOSITED (MeV/g)	MCNP ERROR (Fraction)
701	1.25	2.84	3.503E-14	0.0194
702	5.0	5.61	5.721E-15	0.0203
703	10.0	10.32	1.733E-15	0.0253
704	15.0	15.21	8.100E-16	0.0287
705	20.0	20.16	4.387E-16	0.0313
706	25.0	25.13	2.627E-16	0.0338
707	30.0	30.10	1.680E-16	0.0362
708	35.0	35.09	1.107E-16	0.0383
709	40.0	40.08	7.759E-17	0.0404
710	46.25	46.32	5.083E-17	0.0420
711	55.0	55.06	2.994E-17	0.0453
712	65.0	65.05	1.632E-17	0.0474
713	75.0	75.04	9.595E-18	0.0501
714	85.0	85.03	5.704E-18	0.0523

HEIGHT = 32.5 km

CELL NUMBER	GROUND RANGE (km)	SLANT RANGE (km)	ENERGY DEPOSITED (MeV/g)	MCNP ERROR (Fraction)
601	1.25	7.65	3.759E-15	0.0574
602	5.0	9.05	2.437E-15	0.0311
603	10.0	12.53	1.220E-15	0.0284
604	15.0	16.79	6.650E-16	0.0290
605	20.0	21.38	3.787E-16	0.0314
606	25.0	26.11	2.282E-16	0.0331
607	30.0	30.93	1.394E-16	0.0344
608	35.0	35.81	9.008E-17	0.0345
609	40.0	40.71	5.916E-17	0.0361
610	46.25	46.86	3.771E-17	0.0387
611	55.0	55.52	2.058E-17	0.0438
612	65.0	65.44	1.117E-17	0.0496
613	75.0	75.38	6.175E-18	0.0492
614	85.0	85.33	3.496E-18	0.0513

HEIGHT = 28.75 km

CELL NUMBER	GROUND RANGE (km)	SLANT RANGE (km)	ENERGY DEPOSITED (MeV/g)	MCNP ERROR (Fraction)
501	1.25	11.37	1.735E-15	0.0745
502	5.0	12.35	1.338E-15	0.0387
503	10.0	15.10	8.546E-16	0.0333
504	15.0	18.78	5.247E-16	0.0343
505	20.0	22.97	3.083E-16	0.0378
506	25.0	27.43	1.777E-16	0.0366
507	30.0	32.06	1.154E-16	0.0405
508	35.0	36.78	6.786E-17	0.0421
509	40.0	41.56	4.272E-17	0.0395
510	46.25	47.61	2.674E-17	0.0410
511	55.0	56.15	1.447E-17	0.0432
512	65.0	65.97	7.091E-18	0.0443
513	75.0	75.85	3.865E-18	0.0443
514	85.0	85.75	2.308E-18	0.0487

HEIGHT = 22.0 km

CELL NUMBER	GROUND RANGE (km)	SLANT RANGE (km)	ENERGY DEPOSITED (MeV/g)	MCNP ERROR (Fraction)
301	1.25	18.10	6.732E-16	0.0752
302	5.0	18.73	5.400E-16	0.0425
303	10.0	20.63	4.066E-16	0.0353
304	15.0	23.47	2.534E-16	0.0368
305	20.0	26.94	1.502E-16	0.0374
306	25.0	30.83	8.974E-17	0.0405
307	30.0	35.01	5.221E-17	0.0404
308	35.0	39.38	3.110E-17	0.0387
309	40.0	43.88	1.923E-17	0.0384
310	46.25	49.65	1.171E-17	0.0374
311	55.0	57.88	5.884E-18	0.0367
312	65.0	67.46	2.986E-18	0.0397
313	75.0	77.15	1.611E-18	0.0391
314	85.0	86.90	8.838E-19	0.0402

Appendix C: Table of Atmospheric Number Densities

This appendix contains a reproduction of the tables of number densities of various atmospheric constituents (vs. altitude) which were provided by AFWL/NTN and used in support of this work. (The reproductions are the best quality we could obtain readily.) The tables cover the range from sea level to 800 km altitude.

ALT. (km)	NUMBER DENSITY (cm^{-3})				
	N_2	O_2	O	He	Ar
0	1.989E 19	5.336E 18	3.000E 10	1.335E 14	2.380E 17
1	1.811E 19	4.860E 18	3.674E 10	1.216E 14	2.167E 17
2	1.634E 19	4.384E 18	4.500E 10	1.097E 14	1.955E 17
3	1.481E 19	3.974E 18	6.093E 10	9.944E 13	1.772E 17
4	1.328E 19	3.561E 18	8.250E 10	8.911E 13	1.588E 17
5	1.199E 19	3.216E 18	1.090E 11	8.046E 13	1.434E 17
6	1.070E 19	2.870E 18	1.440E 11	7.182E 13	1.280E 17
7	9.605E 18	2.577E 18	1.859E 11	6.448E 13	1.149E 17
8	8.512E 18	2.283E 18	2.400E 11	5.714E 13	1.018E 17
9	7.614E 18	2.043E 18	3.059E 11	5.111E 13	9.109E 16
10	6.716E 18	1.802E 18	3.900E 11	4.508E 13	8.035E 16
11	5.892E 18	1.581E 18	4.837E 11	3.955E 13	7.049E 16
12	5.069E 18	1.360E 18	6.000E 11	3.402E 13	6.064E 16
13	4.385E 18	1.176E 18	7.470E 11	2.943E 13	5.246E 16
14	3.701E 18	9.930E 17	9.300E 11	2.485E 13	4.428E 16
15	3.202E 18	8.589E 17	1.157E 12	2.149E 13	3.831E 16
16	.702E 18	7.249E 17	1.440E 12	1.814E 13	3.233E 16
17	2.339E 18	6.274E 17	1.764E 12	1.570E 13	2.798E 16
18	1.976E 18	5.300E 17	2.160E 12	1.326E 13	2.364E 16
19	1.710E 18	4.588E 17	2.546E 12	1.148E 13	2.046E 16
20	1.445E 18	3.876E 17	3.000E 12	9.698E 12	1.728E 16
21	1.245E 18	3.341E 17	3.854E 12	8.361E 12	1.490E 16
22	1.046E 18	2.807E 17	4.950E 12	7.024E 12	1.252E 16
23	9.043E 17	2.426E 17	5.780E 12	6.070E 12	1.082E 16
24	7.622E 17	2.045E 17	6.750E 12	5.116E 12	9.119E 15
25	6.591E 17	1.768E 17	7.530E 12	4.424E 12	7.885E 15
26	5.560E 17	1.492E 14	8.400E 12	3.732E 12	6.652E 15
27	4.814E 17	1.292E 17	8.549E 12	3.232E 12	5.760E 15
28	4.068E 17	1.091E 17	8.700E 12	2.731E 12	4.868E 15
29	3.509E 17	9.415E 16	8.849E 12	2.356E 12	4.199E 15
30	2.950E 17	7.915E 16	9.000E 12	1.980E 12	3.530E 15
31	2.523E 17	6.782E 16	8.617E 12	1.697E 12	3.024E 15
32	2.166E 17	5.812E 16	8.250E 12	1.454E 12	2.592E 15
33	1.861E 17	4.992E 16	7.462E 12	1.249E 12	2.226E 15
34	1.600E 17	4.293E 16	6.750E 12	1.074E 12	1.914E 15
35	1.378E 17	3.695E 16	6.037E 12	9.247E 11	1.648E 15
36	1.188E 17	3.186E 16	5.400E 12	7.973E 11	1.421E 15
37	1.025E 17	2.751E 16	4.589E 12	6.883E 11	1.227E 15
38	8.863E 16	2.378E 16	3.900E 12	5.950E 11	1.060E 15
39	7.669E 16	2.057E 16	3.059E 12	5.148E 11	9.176E 14
40	6.648E 16	1.784E 16	2.400E 12	4.463E 11	7.955E 14
41	5.767E 16	1.547E 16	1.990E 12	3.871E 11	6.900E 14
42	5.008E 16	1.344E 16	1.650E 12	3.362E 11	5.992E 14
43	4.354E 16	1.168E 16	1.268E 12	2.923E 11	5.210E 14
44	3.791E 16	1.017E 16	9.750E 11	2.545E 11	4.536E 14
45	3.306E 16	8.869E 15	7.552E 11	2.219E 11	3.955E 14
46	2.885E 16	7.739E 15	5.850E 11	1.936E 11	3.451E 14
47	2.520E 16	6.761E 15	4.492E 11	1.692E 11	3.015E 14
48	2.202E 16	5.908E 15	3.450E 11	1.478E 11	2.635E 14
49	1.928E 16	5.173E 15	2.692E 11	1.294E 11	2.307E 14
50	1.690E 16	4.534E 15	1.917E 11	1.134E 11	2.022E 14
51	1.508E 16	4.045E 15	1.524E 11	1.012E 11	1.804E 14
52	1.343E 16	3.603E 15	1.208E 11	9.016E 10	1.607E 14
53	1.195E 16	3.207E 15	1.010E 11	8.025E 10	1.430E 14
54	1.063E 16	2.851E 15	8.419E 10	7.134E 10	1.272E 14

Fig. 14. Altitude Dependent Atmospheric Number Densities

ALT. (km)	NUMBER DENSITY (cm^{-3}) N_2	O_2	O	He	Ar
55	9.433E 15	2.531E 15	7.238E 10	6.332E 10	1.129E 14
56	8.363E 15	2.244E 15	6.193E 10	5.614E 10	1.001E 14
57	7.406E 15	1.987E 15	5.464E 10	4.972E 10	8.861E 13
58	6.550E 15	1.757E 15	4.801E 10	4.397E 10	7.837E 13
59	5.786E 15	1.552E 15	4.246E 10	3.884E 10	6.922E 13
60	5.103E 15	1.369E 15	3.746E 10	3.426E 10	6.106E 13
61	4.493E 15	1.205E 15	3.493E 10	3.016E 10	5.376E 13
62	3.951E 15	1.060E 15	3.256E 10	2.652E 10	4.727E 13
63	3.469E 15	9.306E 14	3.076E 10	2.382E 10	4.150E 13
64	3.040E 15	8.156E 14	2.912E 10	2.041E 10	3.637E 13
65	2.661E 15	7.140E 14	2.800E 10	1.786E 10	3.184E 13
66	2.327E 15	6.243E 14	2.702E 10	1.562E 10	2.784E 13
67	2.031E 15	5.449E 14	2.618E 10	1.363E 10	2.430E 13
68	1.770E 15	4.749E 14	2.549E 10	1.188E 10	2.118E 13
69	1.539E 15	4.129E 14	2.521E 10	1.033E 10	1.842E 13
70	1.337E 15	3.587E 14	2.505E 10	8.974E 09	1.600E 13
71	1.161E 15	3.115E 14	2.224E 10	7.795E 09	1.389E 13
72	1.007E 15	2.700E 14	2.300E 10	6.757E 09	1.204E 13
73	8.707E 14	2.336E 14	2.469E 10	5.845E 09	1.042E 13
74	7.514E 14	2.016E 14	2.650E 10	5.044E 09	8.990E 12
75	6.474E 14	1.737E 14	2.820E 10	4.346E 09	7.746E 12
76	5.565E 14	1.493E 14	3.000E 10	3.736E 09	6.659E 12
77	4.770E 14	1.280E 14	3.240E 10	3.202E 09	5.707E 12
78	4.082E 14	1.095E 14	3.500E 10	2.740E 09	4.884E 12
79	3.482E 14	9.342E 13	3.742E 10	2.337E 09	4.166E 12
80	2.963E 14	7.950E 13	4.000E 10	1.989E 09	3.545E 12
81	2.478E 14	6.649E 13	4.472E 10	1.663E 09	2.965E 12
82	2.072E 14	5.559E 13	5.000E 10	1.391E 09	2.479E 12
83	1.733E 14	4.648E 13	5.477E 10	1.163E 09	2.073E 12
84	1.449E 14	3.888E 13	6.000E 10	9.725E 08	1.734E 12
85	1.212E 14	3.251E 13	6.753E 10	8.132E 08	1.450E 12
86	1.014E 14	2.721E 13	7.600E 10	6.807E 08	1.213E 12
87	8.480E 13	2.275E 13	8.718E 10	5.691E 08	1.014E 12
88	7.095E 13	1.906E 13	1.000E 11	4.761E 08	8.486E 11
89	5.934E 13	1.598E 13	1.118E 11	3.982E 08	7.098E 11
90	4.965E 13	1.332E 13	1.250E 11	3.332E 08	5.939E 11
91	4.103E 13	1.101E 13	1.449E 11	2.753E 08	4.868E 11
92	3.544E 13	9.188E 12	1.680E 11	2.282E 08	4.046E 11
93	2.831E 13	7.361E 12	2.114E 11	1.886E 08	3.363E 11
94	2.349E 13	6.146E 12	2.660E 11	1.568E 08	2.795E 11
95	1.947E 13	5.190E 12	3.302E 11	1.306E 08	2.329E 11
96	1.626E 13	4.296E 12	4.100E 11	1.091E 08	1.945E 11
97	1.362E 13	3.553E 12	4.436E 11	9.144E 07	1.630E 11
98	1.146E 13	2.936E 12	4.800E 11	7.692E 07	1.371E 11
99	9.673E 12	2.423E 12	4.899E 11	6.492E 07	1.157E 11
100	8.178E 12	1.994E 12	5.000E 11	5.492E 07	9.800E 10
101	6.817E 12	1.644E 12	4.879E 11	4.575E 07	8.154E 10
102	5.704E 12	1.359E 12	4.760E 11	4.421E 07	6.823E 10
103	4.804E 12	1.131E 12	4.391E 11	4.275E 07	5.746E 10
104	4.060E 12	9.443E 11	4.050E 11	4.138E 07	4.857E 10
105	3.453E 12	7.932E 11	3.606E 11	4.008E 07	4.130E 10
106	2.950E 12	6.693E 11	3.210E 11	3.886E 07	3.528E 10
107	2.529E 12	5.665E 11	2.839E 11	3.768E 07	3.025E 10
108	2.174E 12	4.809E 11	2.510E 11	3.656E 07	2.601E 10
109	1.875E 12	4.093E 11	2.241E 11	3.551E 07	2.242E 10

Fig. 14. (Continued)

ALT. (km)	NUMBER DENSITY (cm^{-3}) N_2	O_2	O	He	Ar	H
110	1.620E 12	3.492E 11	2.000E 11	3.450E 07	1.938E 10	
111	1.365E 12	2.903E 11	1.811E 11	3.304E 07	1.633E 10	
112	1.164E 12	2.443E 11	1.640E 11	3.171E 07	1.393E 10	
113	9.983E 11	2.066E 11	1.488E 11	3.048E 07	1.194E 10	
114	8.606E 11	1.757E 11	1.350E 11	2.934E 07	1.029E 10	
115	7.460E 11	1.501E 11	1.235E 11	2.829E 07	8.923E 09	
116	6.513E 11	1.292E 11	1.130E 11	2.731E 07	7.791E 09	
117	5.723E 11	1.119E 11	1.022E 11	2.639E 07	6.846E 09	
118	5.057E 11	9.744E 10	9.250E 10	2.554E 07	6.049E 09	
119	4.478E 11	8.501E 10	8.385E 10	2.474E 07	5.357E 09	
120	4.000E 11	7.500E 10	7.600E 10	2.400E 07	4.500E 09	
130	1.383E 11	2.325E 10	3.650E 10	1.801E 07	1.123E 09	
140	6.302E 10	9.729E 09	2.154E 10	1.481E 07	3.960E 08	
150	3.308E 10	4.746E 09	1.411E 10	1.273E 07	1.670E 08	
160	1.891E 10	2.542E 09	9.817E 09	1.122E 07	7.854E 07	
170	1.147E 10	1.454E 09	7.122E 09	1.006E 07	3.990E 07	
180	7.284E 09	8.737E 08	5.335E 09	9.138E 06	2.150E 07	
190	4.794E 09	5.463E 08	4.099E 09	8.385E 06	1.214E 07	
200	3.249E 09	3.527E 08	3.216E 09	7.760E 06	7.113E 06	
210	2.254E 09	2.336E 08	2.565E 09	7.232E 06	4.296E 06	
220	1.594E 09	1.581E 08	2.075E 09	6.779E 06	2.660E 06	
230	1.146E 09	1.088E 08	1.698E 09	6.385E 06	1.680E 06	
240	8.340E 08	7.596E 07	1.403E 09	6.037E 06	1.079E 06	
250	6.138E 08	5.367E 07	1.168E 09	5.728E 06	7.030E 05	
260	4.558E 08	3.829E 07	9.783E 08	5.449E 06	4.632E 05	
270	3.411E 08	2.755E 07	8.242E 08	5.195E 06	3.082E 05	
280	2.569E 08	1.996E 07	6.975E 08	4.963E 06	2.067E 05	
290	1.945E 08	1.455E 07	5.927E 08	4.749E 06	1.397E 05	
300	1.480E 08	1.066E 07	5.053E 08	4.550E 06	9.491E 04	
320	8.666E 07	5.797E 06	3.702E 08	4.191E 06	4.450E 04	
340	5.137E 07	3.195E 06	2.736E 08	3.873E 06	2.120E 04	
360	3.075E 07	1.779E 06	2.035E 08	3.589E 06	1.023E 04	
380	1.854E 07	9.991E 05	1.522E 08	3.331E 06	4.982E 03	
400	1.125E 07	5.650E 05	1.142E 08	3.097E 06	2.448E 03	
420	6.837E 06	3.200E 05	8.588E 07	2.882E 06	.000E 00	
440	4.189E 06	1.829E 05	6.487E 07	2.685E 06	.000E 00	
460	2.577E 06	1.050E 05	4.913E 07	2.503E 06		.000E 00
480	1.591E 06	6.058E 04	3.729E 07	2.335E 06		.000E 00
500	9.858E 05	3.507E 04	2.836E 07	2.180E 06		8.737E 03
520	6.128E 05	2.038E 04	2.161E 07	2.037E 06		8.588E 03
540	3.821E 05	1.188E 04	1.650E 07	1.903E 06		8.442E 03
560	2.390E 05	6.952E 03	1.262E 07	1.780E 06		8.300E 03
580	1.499E 05	4.081E 03	9.667E 06	1.665E 06		8.162E 03
600	9.428E 04	2.404E 03	7.418E 06	1.558E 06		8.027E 03
620	5.947E 04	1.420E 03	5.701E 06	1.458E 06		7.895E 03
640	3.762E 04	8.417E 02	4.389E 06	1.366E 06		7.766E 03
660	2.386E 04	5.004E 02	3.384E 06	1.280E 06		7.640E 03
680	1.517E 04	2.984E 02	2.613E 06	1.200E 06		7.518E 03
700	9.673E 03	1.785E 02	2.021E 06	1.125E 06		7.397E 03
720	6.184E 03	1.071E 02	1.565E 06	1.055E 06		7.280E 03
740	3.963E 03	6.442E 01	1.214E 06	9.902E 05		7.165E 03
760	2.546E 03	3.887E 01	9.429E 05	9.295E 05		7.052E 03
780	1.640E 03	2.352E 01	7.334E 05	8.729E 05		6.942E 03
800	1.059E 03	1.427E 01	5.713E 05	8.200E 05		6.834E 03

Fig. 14. (Continued)

SECURITY CLASSIFICATION OF THIS PAGE

REPORT DOCUMENTATION PAGE

Form Approved
OMB No 0704-0188

1a REPORT SECURITY CLASSIFICATION UNCLASSIFIED	1b RESTRICTIVE MARKINGS
2a SECURITY CLASSIFICATION AUTHORITY	3 DISTRIBUTION / AVAILABILITY OF REPORT Approved for public release; distribution unlimited.
2b DECLASSIFICATION / DOWNGRADING SCHEDULE	
4 PERFORMING ORGANIZATION REPORT NUMBER(S) AFIT/EN-TR-90-5	5 MONITORING ORGANIZATION REPORT NUMBER(S)
6a NAME OF PERFORMING ORGANIZATION Air Force Institute of Technology 6b OFFICE SYMBOL (If applicable) AFIT/ENP	7a NAME OF MONITORING ORGANIZATION
6c ADDRESS (City, State, and ZIP Code) Wright-Patterson AFB OH 45433-6583	7b ADDRESS (City, State, and ZIP Code)
8a NAME OF FUNDING / SPONSORING ORGANIZATION Weapons Laboratory 8b OFFICE SYMBOL (If applicable) WL/NTN	9 PROCUREMENT INSTRUMENT IDENTIFICATION NUMBER
8c ADDRESS (City, State, and ZIP Code) Kirtland AFB NM 87117	10 SOURCE OF FUNDING NUMBERS PROGRAM ELEMENT NO. / PROJECT NO. / TASK NO / WORK UNIT ACCESSION NO.

11 TITLE (Include Security Classification)
Monte Carlo Simulation of Atmospheric Neutron Transport at High Altitudes Using MCNP

12 PERSONAL AUTHOR(S) Culp, Donald Roger; Monti, David Louis; Shoemaker, James Richard; Wesley, David NMN; Mathews, Kirk Alan.

13a TYPE OF REPORT	13b TIME COVERED	14 DATE OF REPORT (Year, Month, Day)	15 PAGE COUNT
Technical	FROM _____ TO _____	1990, August	62

16 SUPPLEMENTARY NOTATION

17 COSATI CODES			18 SUBJECT TERMS (Continue on reverse if necessary and identify by block number)
FIELD	GROUP	SUB-GROUP	Neutron Transport Theory, Atmospheric Attenuation

19 ABSTRACT (Continue on reverse if necessary and identify by block number)

Neutron transport calculations were performed using the Monte Carlo code, MCNP The transport problem considered has a point source at high altitude (40 km). Since atmospheric density decreases with altitude, two-dimensional effects (cylindrical coordinates) can be important. Results were compared to those obtained with the SMAUG-II computer code, which performs mass-integral scaling of approximate fits to one-dimentional spherical discrete ordinates solutions. These comparisons show the importance of two-dimensional computations. The report discusses practical issues of applying MCNP to this problem, without code modifications and includes example input files for MCNP and for SMAUG-11.

20 DISTRIBUTION / AVAILABILITY OF ABSTRACT	21 ABSTRACT SECURITY CLASSIFICATION
☒ UNCLASSIFIED/UNLIMITED ☐ SAME AS RPT ☐ DTIC USERS	UNCLASSIFIED
22a NAME OF RESPONSIBLE INDIVIDUAL LCDR Kirk A. Mathews, USN	22b TELEPHONE (Include Area Code) (513)748-9841 22c OFFICE SYMBOL AFIT/ENP

DD Form 1473, JUN 86 *Previous editions are obsolete.* SECURITY CLASSIFICATION OF THIS PAGE